Single-Crystal Elastic Properties of Geomaterials

Im Fachbereich Geowissenschaften der Freien Universität Berlin eingereichte Dissertation von

Dipl. Min. Hauke Marquardt

2009

Gutachter:

Prof. Frank R. Schilling (Freie Universität Berlin)

Prof. Susan Schorr (Freie Universität Berlin)

Tag der letzten mündlichen Prüfung (Disputation): 02.07.09

Ich möchte mich bei einer Reihe von Mitstreitern, Freunden und Bekannten bedanken, ohne deren Unterstützung die vorliegende Arbeit niemals so wäre wie sie ist.

Anfangen möchte ich bei Frank Schilling, dem ich für die Organisation und Betreuung der Doktorarbeit danke. Ich danke ihm für zahlreiche Diskussionen über die Themen dieser Arbeit und insbesondere auch dafür, dass er mir immer „freie Hand“ gelassen hat und stets meine Vorhaben und Wünsche unterstützt hat.
Ganz besonders möchte ich mich bei Sergio Speziale für die hervorragende Betreuung meiner Arbeit bedanken. Er war immer bereit mir ausgiebig mit Rat und Tat zur Seite zu stehen und hat meine Ideen und Vorstellungen stets respektiert. Die Arbeit mit Sergio hat mir sehr viel Spaß bereitet und diese Freude war nicht zuletzt für den zügigen Fortschritt und Erfolg dieser Arbeit verantwortlich. Vielen Dank!
Auch möchte ich Hanni Reichmann herzlich danken, der ebenfalls meine Arbeit betreut hat und stets sehr am Fortschritt meiner Projekte interessiert war. Außerdem danke ich Hanni für die vielen kleinen netten Gespräche zwischen „Tür und Angel“.
Wilhelm Heinrich möchte ich für seine stetige Unterstützung und insbesondere für die „Karriereplanung“ danken.
Susan Schorr danke ich für Ihre Bereitschaft als Zweitgutachterin zu agieren.
Besonders danken möchte ich auch Dan Frost, der den Ferroperiklas zur Verfügung gestellt hat und Ed Garnero, der mir einige interessante „Seismologenaspekte“ näher gebracht hat und durch seine freundlichen, amüsanten Emails meine Laune so manches Mal gehoben hat.
Fabio Cammarano danke ich für seine Interesse an meinen Ergebnissen und sein schnelles Feedback (und den Kaffee auf der AGU).
Für zahlreiche interessante Gespräche über diese Arbeit und für ihre Korrekturvorschläge danke ich Katharina Hartmann. Weitere interessante Diskussionen habe ich Sandro Jahn, Monika Koch-Müller und Christian Schmidt zu verdanken.
Bei Monika möchte ich mich auch ausdrücklich dafür bedanken, dass sie sich die Zeit für IR-Messungen meiner Probe genommen hat.
Matthias Gottschalk und Tiziana Boffa Ballaran danke ich für die Einkristalldiffraktometrie, Steffen Ganschow für die Synthese der synthetischen Granatkristalle.
Für „technische“ Unterstützung am GFZ möchte ich mich bei Beate Hein, Andreas Ebert, Heike Steigert, Reiner Schulz, Gerhard Berger, Onna Appelt und Dieter Rhede bedanken.
Meine Arbeiten am Synchrotron wurden tatkräftig und freundlich von Heribert Wilhelm (Diamond Light Source) und Innokenty Kantor, Vitali Prakapenka und Stanislav Sinogeikin (Advanced Photon Source) unterstützt – vielen Dank dafür. Danke auch an Anastasia Kantor für ihre aufmunternden Worte.
Sylvia-Monique Thomas danke ich für ihre Gastfreundschaft und die Taxifahrt zum APS.
Für ihr Ideen, Vorschläge und Kommentare zu meiner Arbeit möchte ich mich bei “Afu” Lin, Thomas Duffy und Raymond Jeanloz bedanken.
Anke Watenphul und Fiorenza Deon waren immer nette „Mitbewohner“ am GFZ und ich danke Ihnen insbesondere für ihre „Kaspar-Toleranz“.
Danke Kaspar für Deine Welterkundungen, die ständig für Aufmunterung und Lachen sorgen.

Mein allergrößter Dank gilt Tinka!

Single-Crystal Elastic Properties of Geomaterials

1. Summary

Elastic properties determine the response of materials to strains within the elastic limit. They reflect the nature of atomic bonding (strength) and carry crucial information about materials' physical and chemical behaviour. This motivates the strong interest in elasticity of several scientific disciplines, including materials sciences, solid state physics, geosciences and chemistry. A quantitative understanding of elastic properties and elastic wave velocities in the minerals that likely compose the deep Earth is of central importance for geosciences as it facilitates the interpretation of seismological observations in terms of composition, evolution, dynamics and thermal state of the Earth's interior. This thesis contributes to this key challenge by extending our knowledge of how elastic properties change with chemical composition, pressure, and temperature and how these findings relate to seismological observables.

Chapter 2 provides a brief introduction to the structure, mineralogy, dynamics and thermal state of the deep Earth and illustrates the motivation for the present research. Chapter 3 outlines the theory of elasticity and summarizes important relationships between elastic properties and the propagation of sound waves in both single-crystals and mineral aggregates. The treatment of elastic properties at high-pressures within the framework of finite strain theory will be briefly described. The chapter concludes with an overview of commonly used techniques to study the elastic behaviour of materials at high-pressures and high-temperatures. Chapter 4 describes the experimental methods used in this thesis. The introduction to diamond-anvil cells, which were employed to generate the extreme pressures of the deep Earth, is followed by a discussion of the two main techniques used for the present research - Brillouin scattering and x-ray diffraction.

The findings of this thesis are discussed in chapter 5 and 6. The main results and implications are presented in the form of extended abstracts (chapter 5), which are supplemented by the complete manuscripts in chapter 6.

The first part (5.1, 5.2, 5.3) of the discussion is dedicated to the pressure-, temperature-, and compositional-dependence of the elasticity of single-crystal (Mg,Fe)O ferropericlase, the second most abundant mineral of Earth's lower mantle. It has recently been shown that the octahedrally coordinated Fe^{2+} in ferropericlase undergoes a spin transition at lower mantle

pressures. This modification of electronic configuration is accompanied by changes in several physical properties, including elasticity (Marquardt et al. 2009c; Marquardt et al. 2009d).

Chapter 5.1 reports the effect of the pressure-induced spin transition on the elastic properties of ferropericlase and discusses the implications for the interpretation of both one-dimensional and three-dimensional seismic models. The major finding is that the spin-transition lowers compressional wave velocities, but does not affect shear velocities. This leads to significant perturbations of the velocity ratios and their dependence on pressure, temperature, and iron content. If these mechanisms are well understood and future seismological studies succeed to resolve its elastic signature, the spin transition could provide important constraints on both temperature and iron distribution in Earth's mid-lower mantle (Marquardt et al. 2009c).

Chapter 5.2 focuses on the significance of (Mg,Fe)O for the interpretation of seismic anisotropy observations in the lowermost mantle. Here, the main conclusion is that (Mg,Fe)O likely dominates seismic anisotropy in the lower mantle, even though it composes only ~20 Vol.% of this region. This implies that seismic anisotropy could also be present above the D'' discontinuity, where seismologists depict it, in regions where deformation is dominated by dislocation creep at very high strain levels. These findings can affect our understanding of Earth's mantle flow and dynamics (Marquardt et al. 2009d).

Chapter 5.3 presents results on the effect of temperature on the elastic constants of (Mg,Fe)O at high pressures. The data indicate that increasing temperature generally lowers average velocities, particularly shear velocities, but it also markedly influences the elastic shear anisotropy. Increasing the temperature leads to stronger elastic shear anisotropy at pressures below ~20 GPa, but lowers shear anisotropy at pressures corresponding to the lower mantle. These first results on the elasticity of ferropericlase at simultaneously high-pressure and high-temperature provide a basis for future studies to experimentally quantify the elastic tensor at mantle conditions.

In the second part of chapter 5 (5.4, 5.5), the effect of chemical substitution on the elastic tensor of both synthetic and natural garnet solid solution series is discussed. Silicate garnets are major components in Earth's crust and upper mantle, especially in the transition zone. Moreover, members of the garnet group are important compounds in materials science, because they are well suited for a variety of technological applications, such as solid state lasers.

Chapter 5.4 outlines the single-crystal elastic properties of synthetic garnets that belong to the $Y_3Al_5O_{12}$-$Yb_3Al_5O_{12}$ solid solution series. The elastic tensor was derived from Brillouin scattering and is complemented by computational results. The data show that the substitution of yttrium by the smaller and heavier ytterbium makes the material stiffer (the bulk modulus increases), but does not affect its elastic shear properties. These results can help to better understand elasticity-composition systematics in isostructural natural garnet solid-solution series and, furthermore, to elucidate the potentials and limitations of computational approaches (Marquardt et al. 2009b).

Chapter 5.5 discusses the elastic properties of natural garnets and relates them to the systematics observed for the synthetic solid solution series. The main outcome is that cation substitution in the studied natural garnet solid solution series produces effects that are comparable to the observations for the synthetic one, where the incompressibility varies, but the shear properties remain unchanged. These findings suggest that elasticity systematics are, at least to some extent, transferable between different garnet solid solution series and might also be applicable to majorite-pyrope garnet, which is probably the most abundant single mineral phase in Earth's transition zone.

2. The Earth's Mantle

The major part of this thesis focuses on the lower mantle mineral phase ferropericlase and the implications of its elastic properties for the interpretation of geophysical observations. In addition, the elastic properties of members of the garnet group are discussed, which are major components of the upper mantle, particularly the transition zone. This chapter provides a brief summary of our present knowledge of the structure, mineralogy, dynamics and thermal state of the deep Earth and the role of mineral physics.

The Earth's mantle plays a pivotal role in the evolution and dynamics of our planet. The large convective regime of Earth's mantle manifests itself through plate tectonics and affects life on our planet, for instance through earthquakes and volcanic eruptions. Exploring the deep Earth is thus not simply an academic curiosity, but a major challenge towards a more complete understanding of the processes that determine the dynamics of our planet and the implications for life on its surface. Unfortunately, direct probing of Earth's mantle by far exceeds our present capabilities - drilling campaigns are limited to about 12.3 km depth, which is about 1/500 from the surface to the centre of our planet.

To date, interpretation of the behaviour of seismic waves inside the Earth provides the most complete picture of the structure, mineralogy, and dynamics of the inaccessible interior (e.g. Cammarano et al. 2005; Romanowicz 2008). Inversion of seismic data in terms of radial density/velocity-depth profiles, for instance seismic reference models PREM (Dziewonski and Anderson 1981) or ak135 (Kennett et al. 1995), revealed (more or less) abrupt changes in seismic velocities at defined depths, and lead to the commonly accepted idea that the Earth consists of shells with distinct physical properties (fig. 2.1).

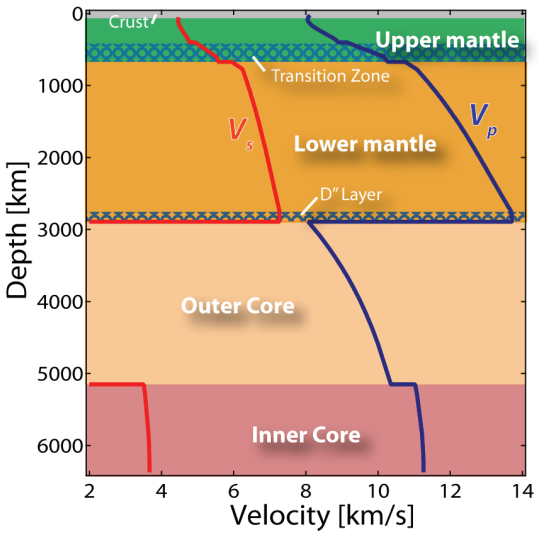

Fig. 2.1: Preliminary Reference Earth Model (PREM) (Dziewonski and Anderson 1981). Average shear and compressional velocities show discontinuities at certain depths, which are often associated with structural changes of the minerals that compose the Earth.

However, a number of seismic tomography studies (Thurber and Ritsema 2007) show that there are significant variations in wave speeds at given depths (lateral heterogeneities) (e.g. Su and Dziewonski 1997; Masters et al. 2000), which are usually quantified in terms of deviations from a one-dimensional reference model, such as PREM. These lateral heterogeneities can be attributed to variations in temperature, chemical composition, or phases (e.g. Karato and Karki 2001; Stixrude and Lithgow-Bertelloni 2007).

To extract information about the actual temperature (fig. 2.2), mineralogy (fig. 2.3) and dynamics of the deep interior from seismic observables (both 1-D and 3-D), constraints on physical properties of deep Earth phases are needed (e.g. Garnero and McNamara 2008). Particularly, mineral physics information about sound wave velocities of candidate mantle minerals under relevant pressure (P) and temperature (T) conditions are essential. Even though recent experimental developments made it possible to reach the P/T-conditions of Earth's core (Dubrovinsky et al. 2007), measuring sound wave velocities in-situ is still very challenging and to date, the very few experimental data sets are mostly limited to upper mantle P/T-conditions (Chen et al. 1998; Li et al. 1998; Liu et al. 2005; Gwanmesia et al. 2006; Sinogeikin et al. 2006; Gwanmesia et al. 2008; Higo et al. 2008). Computational studies were performed on the most relevant lower mantle phases (Karki et al. 1999; Wentzcovitch et al. 2004; Stackhouse et al. 2005; Wentzcovitch et al. 2006), but are usually restricted to iron free systems, due to difficulties in describing the complex electronic structure of transition metals. However, some first partial results, where the thermal contribution has been treated with a thermodynamic approach, have been reported (Tsuchiya et al. 2006b; Koci et al. 2007; Da Silva et al. 2008; Umemoto et al. 2008). Chapter 3.4 gives a brief overview of possible approaches used to determine elasticity at high-pressures and high-temperatures.

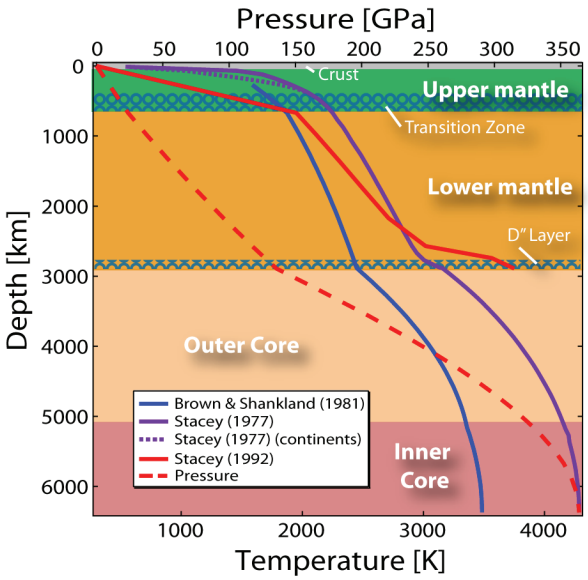

Fig. 2.2: Temperature and pressure as a function of depth in Earth's interior. The pressure is well defined (Dziewonski and Anderson 1981), but large uncertainties remain in the temperature distribution, even in the upper mantle (Frost 2008) as illustrated by the discrepancy between different proposed geotherms (Stacey 1977; Brown and Shankland 1981; Stacey 1992).

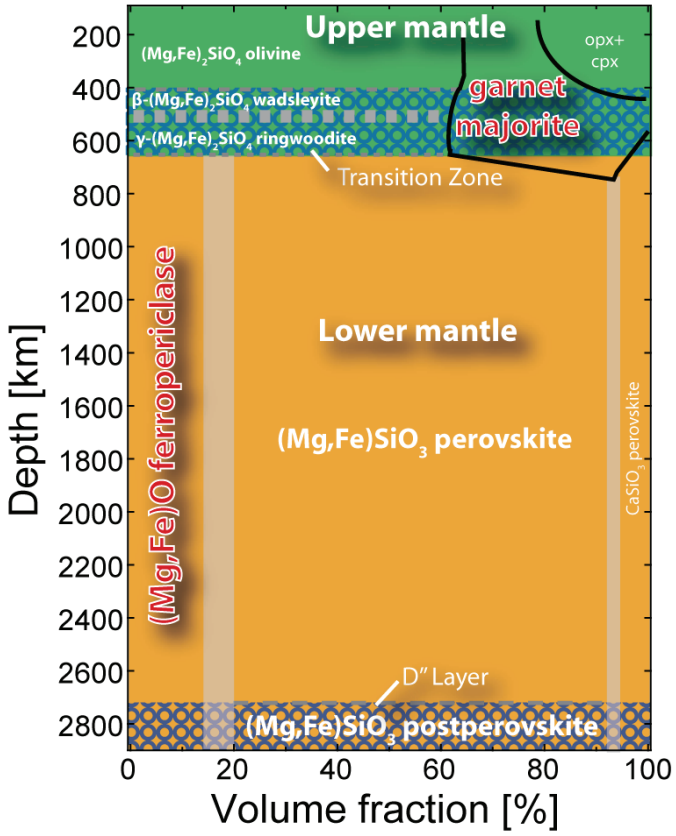

Fig. 2.3: Mineralogical model (pyrolite; Ringwood 1975) of Earth's mantle (adapted from Bina et al. 2003). With increasing depth, the expected mineralogy of Earth's mantle simplifies to mainly two phases, the oxide (Mg,Fe)O ferropericlase and the silicate $(Mg,Fe)SiO_3$ perovskite. At the very bottom of the lower mantle perovskite transforms to post-perovskite (Murakami et al. 2004; Oganov and Ono 2004), which might cause changes in seismic velocities as observed by seismology (Hutko et al. 2008). The most abundant single mineral phase in the transition zone is probably $Mg_3(Fe^{2+},Si,Al)_2Si_3O_{12}$ majorite-pyrope garnet, which is isostructural to the garnets studied in chapter 5.1.3 and 5.1.5.

Iron is particularly important in lower mantle phases, as it has been recently shown that a change in electronic configuration of iron occurs in all major lower mantle phases, including (Mg,Fe)O ferropericlase (Badro et al. 2003; Lin et al. 2007), $(Mg,Fe)SiO_3$ perovskite (Badro et al. 2004; Lin et al. 2008; McCammon et al. 2008a), and post-perovskite (Lin et al. 2008) at lower mantle conditions. This high-spin (HS) to low-spin (LS) transition involves a pairing of the *3d*-electrons in the energetically low lying orbitals (fig. 2.4), but the main cause and the correct thermodynamic description are still under discussion (e.g. Keppler et al. 2007). The possibility of such a transition in mantle minerals was already proposed by Fyfe 1960, but it took more than 40 years of experimental developments until it was finally observed. Iron in LS configuration has a smaller ionic radius than its HS counterpart [LS Fe^{2+}: 0.7-0.72 Å (Fei et al. 2007b), HS Fe^{2+}: 0.78 Å (Shannon 1976)] and thus the spin transition is accompanied by a volume change of the host mineral (Lin et al. 2005a; Tsuchiya et al. 2006b; Speziale et al. 2007a; Fei et al. 2007b; Stackhouse et al. 2007). It has also been shown that the spin transition affects sound wave propagation characteristics of (Mg,Fe)O (Lin et al. 2006; Crowhurst et al. 2008; Marquardt et al. 2009d) but the implications for the interpretation of seismic observations are still under discussion (e.g. Marquardt et al. 2009c; Marquardt et al. 2009d). However, the vast majority of the studies to characterize the physical properties across the

spin-transition have been performed at mantle pressures but ambient temperature. It has been shown both theoretically and experimentally that temperature broadens the pressure range over which the spin transition occurs (Sturhahn et al. 2005; Tsuchiya et al. 2006b; Lin et al. 2007). This makes it unlikely that the spin transition causes abrupt changes, but rather favors gradual changes in physical properties throughout the lower mantle. The potential effects of the iron spin transition in ferropericlase on the elastic signature of the lower mantle are discussed in chapter 5.1.

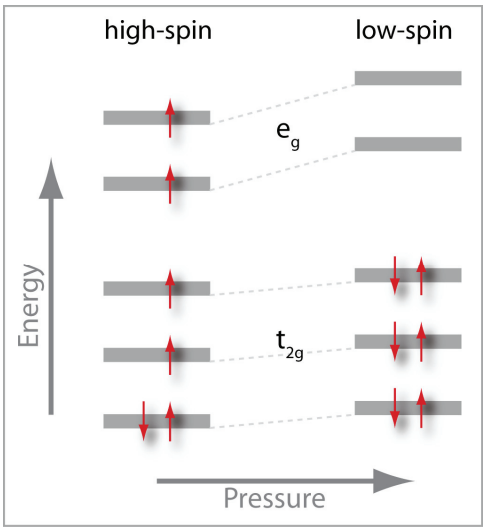

Fig. 2.4: Fe^{2+} in octahedral coordination is subject to crystal field splitting of the five *3d* orbitals caused by the surrounding ligand field. At ambient conditions, the 3d-electrons occupy all five orbitals following Hund's rule. Increasing pressure has more sensible effect on the energy of the e_g orbitals (pointing towards the nearest neighbour oxygens) than on the energy of the t_{2g} orbitals (pointing between the nearest neighbour oxygens). This leads to a pairing of the electrons in the t_{2g} orbitals at a pressure of ~35-100 GPa (Lin and Tsuchiya 2008) in ferropericlase (at 300 K).

In addition to average seismic velocity profiles (fig. 2.1), seismologists depict seismic anisotropy, the direction (or polarization) dependence of seismic propagation speeds, in all parts of the Earth (e.g. Hess 1964; Lay et al. 1998; Vinnik et al. 1998; Fischer 2002; Panning and Romanowicz 2004; Garnero et al. 2004; Panning and Romanowicz 2006; Garnero and McNamara 2008) (fig. 2.5). Seismic anisotropy is thought to be caused by either shape (Kendall and Silver 1996) or lattice preferred orientation (LPO) of the constituent minerals (McNamara et al. 2002). LPO of minerals is induced by dislocation creep and is thus related to deformation processes. Consequently, seismic anisotropy observations, combined with mineral physics constraints on elastic anisotropy and deformation behaviour of Earth materials, can provide insights into dynamic processes in the deep Earth (Zhang and Karato 1995; Mizukami et al. 2004; Wenk et al. 2006; Long et al. 2006; Walte et al. 2009). The elastic anisotropy of ferropericlase at lower mantle pressures is presented in chapter 5.2 along

with a discussion of its implications for seismic observations of anisotropy in the lowermost mantle (for historical reasons[1] called D'' layer) (Marquardt et al. 2009d).

To date, however, there is no experimental technique capable of measuring the elastic tensor at the pressure- and temperature-conditions prevalent throughout Earth's mantle. But recent developments in high-pressure/high-temperature Brillouin scattering experiments in combination with synchrotron x-ray diffraction measurements (Sinogeikin et al. 2007; Murakami et al. 2008, this thesis) are very auspicious. First results on the single-crystal elasticity of ferropericlase measured at simultaneously high-pressures and high-temperatures are presented in chapter 5.3.

Future developments in experimental and computational mineral physics, combined with the recent rapid spreading of seismic receivers around the globe, promise to substantially improve our understanding of Earth's deep interior.

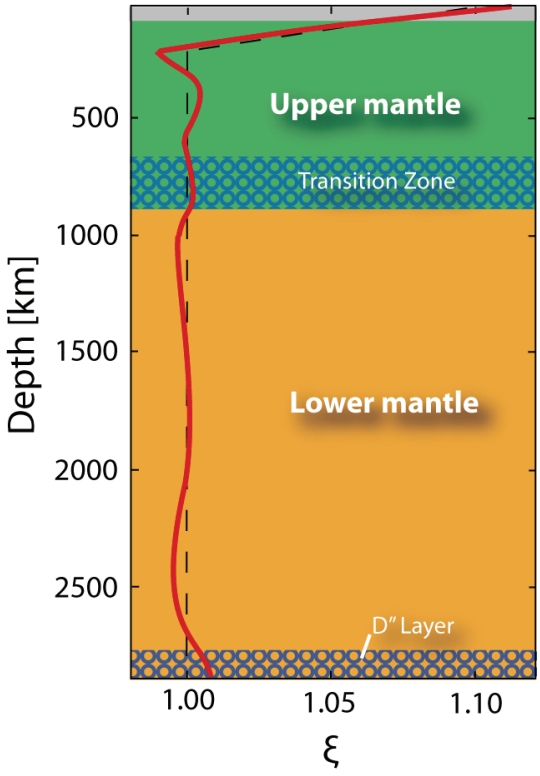

Fig. 2.5: Average seismic shear anisotropy $\xi = V_{SH}^2/V_{SV}^2$ (where V_{SH} and V_{SV} refer to the horizontally and vertically shear wave polarization) in Earth's Interior (modified from Panning and Romanowicz 2006). With the exception of its lowermost part (D'' layer), the lower mantle appears to behave elastically isotropic, at least in average. However, large uncertainties in the depth distribution of anisotropy remain (e.g. Wenk et al. 2006).

[1]Bullen (Bullen, K. E. (1947). An Introduction to the Theory of Seismology, Cambridge University Press.) divided the Earth in seven distinct regions and labelled them with the capital letters A-G, where the D region ranges from a depth of 980km to 2900km; this corresponds roughly to what is known as lower mantle today. However, two years later, Bullen (Bullen, K. E. (1949). Compressibility-Pressure Hypothesis and the Earth's Interior. *Geophys. J. Int.* **5**: 335-368.) discovered that the lowermost part of the D division shows an anomalously low velocity gradient and further divided D into D' and D''.

3. Elasticity

This chapter provides a brief introduction to the elastic properties of solids and their relation to sound wave velocities, more detailed treatments can be found elsewhere (e.g. Karki et al. 2001). Some specific aspects will be discussed for the special case of cubic symmetry, which applies for both ferropericlase (face centered cubic) and garnets (body centered cubic).

3.1. Elastic Properties and Acoustic Waves

Two types of acoustic (sound) body waves can propagate through any solid material, one kind of wave is called longitudinal (or compressional), where the particles oscillate parallel to the propagation direction. The other type is termed transverse (or shear) wave, where the particles oscillate mainly perpendicular to the propagation direction (fig. 3.1). Compressional waves are faster than shear waves and they are therefore called p-waves (primary) in seismology, transverse waves are referred to as S-waves (secondary). Sound wave velocities are related to the elastic moduli and density of a material. In the special case of an elastically isotropic material (for instance a rock without texture), average compressional v_p, shear v_s, and bulk sound velocity v_Φ can be computed from shear G and (adiabatic) bulk modulus K_s (e.g. Poirier 1991; Karki et al. 2001) according to the following identities:

$$v_p = \sqrt{\frac{K_s + \frac{4}{3}G}{\rho}}; \qquad v_s = \sqrt{\frac{G}{\rho}}; \qquad v_\Phi = \sqrt{\frac{K_s}{\rho}} \tag{3.1}$$

The shear modulus (or rigidity) describes the response of a material to shear stress. The bulk modulus (or incompressibility) measures the resistance of a material against a change of volume and is defined as (e.g. Poirier 1991):

$$K = -V\frac{dP}{dV} \tag{3.2}$$

According to its definition, the bulk modulus can be determined by applying an increment of pressure to a material and measuring the corresponding change in volume, i.e. the (isothermal) bulk modulus can be calculated from x-ray diffraction experiments carried out at

high pressures (e.g. Marquardt et al. 2009c). In experiments where a static pressure is applied and the resulting change of volume is monitored, the energy change (heat) associated with the compression can equilibrate and the measured bulk modulus is isothermal. In case of experimental techniques that measure processes that are "faster" than the time needed for the specimen to reach thermal equilibrium, such as Brillouin spectroscopy, one obtains adiabatic moduli. Adiabatic bulk modulus K_S and isothermal bulk modulus K_T are related by the identity $K_S = K_T(1+\alpha\gamma T)$, where α is the volumetric thermal expansion coefficient and γ is the Grüneisen parameter (e.g. Anderson and Isaak 1995). Adiabatic and isothermal shear modulus are equal (for symmetries higher than monoclinic).

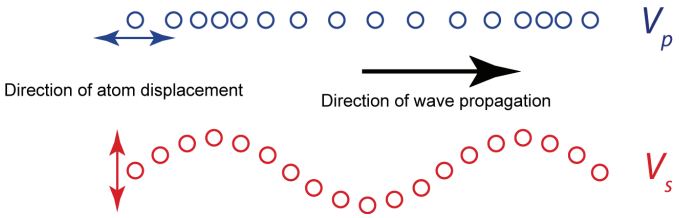

Fig. 3.1: Illustration of particle displacement (polarization) of a transverse (or shear, s-) and a longitudinal (or compressional, p-) wave moving to the right.

In the general anisotropic case of minerals, elastic properties are usually described by the elastic tensor. The elastic stiffness tensor relates stress (force per unit area) to strain (change in length per unit length) by the generalized Hooke's Law (e.g. Nye 1985)[2].

$$\sigma_{ij} = c_{ijkl} \cdot \varepsilon_{kl} \qquad (3.3)$$

Both stress σ_{ij} and strain ε_{kl} are second rank (field) tensors, where the first subscript gives the direction of force or displacement and the second subscript refers to the normal to the face on which the force acts or deformation occurs (fig. 3.2). Therefore, the elastic stiffness tensor c_{ijkl} is a fourth rank (property) tensor containing 81 components (Nye 1985). It appears that stress and strain tensors are both symmetric, because static equilibrium is required (no translation or rotation), which reduces the 81 independent components of the elastic stiffness tensor to 36. The number of independent components further reduces to 21 by considering energetic arguments (Nye 1985). These requirements allow for expressing the elastic tensor components in a simplified Voigt (Voigt 1928) notation, where the four indices are rewritten according to the following conventions: 11->1, 22->2, 33->3, 23-> 4, 31-> 5, 12-> 6. c_{ii} with

[2] Einstein summation notation applies

$i \leq 3$ are called longitudinal constants, whereas c_{ii} with $i \geq 4$ are shear constants, c_{ij} (with $i \neq j < 3$) are referred to as off-diagonal constants.

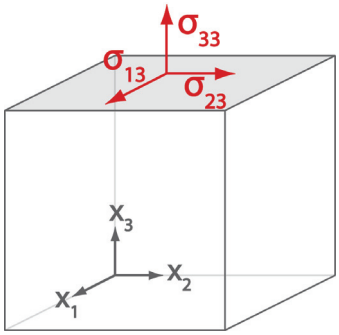

Fig. 3.2: Illustration of the stress tensor components σ_{ij} (the same conventions apply to the strain tensor).

Crystallographic symmetry further reduces the number of independent components. The case of an elastically isotropic material, where the elastic response is fully given by two elastic moduli, e.g. the bulk and the shear modulus, was outlined before. For crystals of cubic symmetry, the elastic properties are described by the three independent non-zero constants c_{11}, c_{12}, and c_{44} in Voigt notation (Nye 1985); figure 3.3 illustrates the meaning of the three elastic constants in the cubic case. Because elastic behaviour is determined by a fourth rank tensor, elastic anisotropy can be found for all crystals, regardless of symmetry.

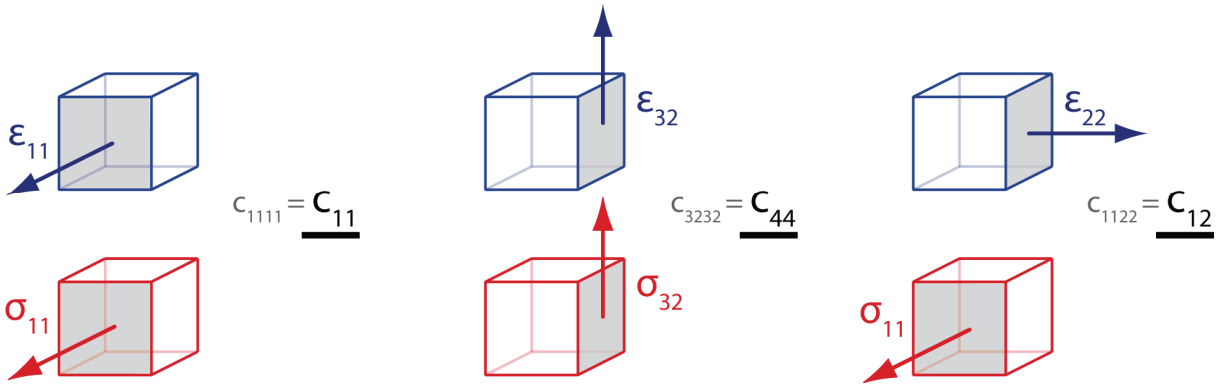

Fig. 3.3: Illustration of the three independent elastic constants in case of cubic symmetry. c_{11} is referred to as longitudinal constant, c_{44} is the shear constant, and c_{12} is called off-diagonal.

By combining eq. (3.3) with the plane wave solution of the equation of motion for propagating elastic waves, one can derive the Christoffel equation, which relates wave velocity v, polarization, and elastic tensor components c_{ijkl} along a given propagation direction n_i (e.g. Musgrave 1970; Karki et al. 2001; Newnham 2005):

$$\det\left|c_{ijkl} n_j n_l - \rho v^2 \delta_{ik}\right| = 0 \qquad (3.4)$$

where δ_{ik} is the Kronecker delta. This equation has three solutions (i = 1, 2, 3): One quasi-longitudinal wave, and two quasi-shear waves (e.g. Karki et al. 2001). Pure longitudinal or shear-waves are only found in elastically isotropic materials or along high-symmetry directions (e.g. Karki et al. 2001). The dependence of wave velocities on propagation direction, and polarization in the case of shear waves, is illustrated in figure 3.4 for $(Mg_{0.9}Fe_{0.1})O$ ferropericlase (Marquardt et al. 2009c; Marquardt et al. 2009d). It follows from eq. (3.4) that the complete set of elastic constants can be determined by measuring sound wave velocities with different polariations and propagation directions when the density of the sample is known.

Numerous definitions of elastic anisotropy are used in the literature. For the interpretation of seismic observations it is convenient to define elastic anisotropy A as:

$$A = \frac{v_{i,\max} - v_{i,\min}}{\left(v_{i,\max} + v_{i,\min}\right)/2} \qquad (3.5)$$

where $v_{i,max}$ and $v_{i,min}$ correspond to maximum and minimum velocity. The subscript i can be substituted by “p” (for compressional wave anisotropy) or “s” (for shear wave anisotropy). This is the general definition for azimuthal anisotropy, in case of shear wave polarization anisotropy, $v_{i,max}$ and $v_{i,min}$ are maximum and minimum shear velocity in a given direction. For cubic symmetry, the maxima of azimuthal and polarization shear anisotropy are equal.

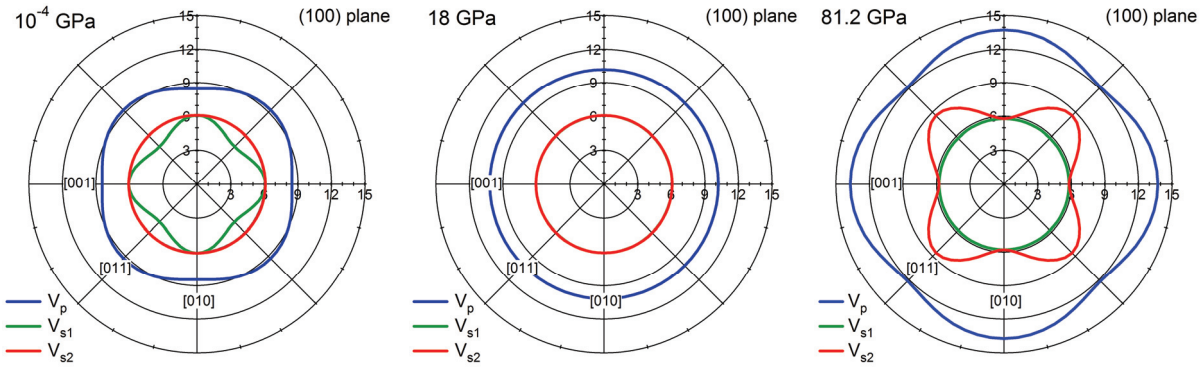

Fig. 3.4: Direction and polarization dependence of the sound wave velocites in ferropericlase at different pressures. Polar plots represent (100) plane, special crystallographic directions are indicated. At ambient pressure, ferropericlase shows consiberable elastic anisotropy (left). With increasing pressure the anisotropy decreases, but after passing through elastic isotropy at around 18 GPa (middle), ferropericlase becomes strongly anisotropic again (with reversed sign) at 81.2 GPa, a pressure corresponding to the middle of Earth's lower mantle (~24-136 GPa). Note that the fastest shear wave is always defined as v_{s2}.

3.2. Elasticity of Aggregates

The Earth is made up of mineral assemblages (rocks) and averaging schemes are needed to relate experimentally determined single-crystal elastic properties of candidate minerals to the large-scale elastic properties measured by seismology. The average elastic properties (bulk and shear modulus) of an isotropic monophase aggregate (randomly oriented grains) are restricted to lie between two bounds, representing either uniform stress (Reuss 1929) or uniform strain (Voigt 1928) throughout the aggregate. Usually, the arithmetic mean (Voigt-Reuss-Hill average) of these two bounds is taken to best approximate the aggregate elasticity (Hill 1952). In the special case of cubic symmetry, the bulk modulus is identical for both bounds and given by:

$$K = \frac{1}{3}\left(c_{11} + 2c_{12}\right) \qquad (3.6)$$

The boundaries for the average shear modulus can be calculated from the two cubic shear constants c_{44} and $c_s = (c_{11}\text{-}c_{12})/2$:

$$G_{\mathrm{Re}uss} = 5/\left(\frac{4}{c_s^{\,2}} + \frac{3}{c_{44}}\right) \quad ; \qquad G_{Voigt} = \frac{1}{5}\left(c_s^{\,2} + 3c_{44}\right) \tag{3.7}$$

Another widely used averaging scheme, particularly for high-symmetry crystals, with tighter bounds is the Hashin-Shtrikman model (Hashin and Shtrikman 1962). Watt 1988 gives a detailed discussion about advantages and disadvantages of averaging models.

The aggregate bulk and shear moduli can then be used to calculate average shear, compressional and bulk velocities (eq. 1) that can be related to one-dimensional radial seismic models, such as PREM (Dziewonski and Anderson 1981) or ak135 (Kennett et al. 1995). Note that mineral aggregates appear elastically isotropic only if the wavelength of the traversing sound wave is much larger than the grain size and if the grains are statistically oriented, which is not necessarily true. Deformation processes, for instance, can cause texturing of aggregates (lattice preferred orientation), which then adopts the anisotropic elastic properties of the constituent minerals. In this case, information about texturing, along with the single-crystal elastic constants, is required to calculate the elastic properties of the aggregate (e.g. Mainprice and Humbert 1994).

3.3. Elasticity at High Pressures – Equation of State

The Equation of State (EoS) of a substance gives the pressure as a function of volume and temperature (e.g. Slater 1963; Anderson 1989). An isothermal Equation of State (EoS) is usually used to describe and extrapolate experimental data, such as $P(V)$ data from x-ray diffraction, collected at high-pressures and ambient temperatures. The most widely applied Equation of State in geophysics is the Birch-Murnaghan EoS, which was developed in the framework of the Eulerian finite strain theory (Murnaghan 1937; Birch 1938; Davies 1974) and is based on the expansion of the Helmholtz free energy F in powers of the Eulerian finite strain f, which is defined as:

$$f = \frac{1}{2}\left[\left(\frac{\rho}{\rho_0}\right)^{2/3} - 1\right] \tag{3.8}$$

where ρ and ρ_0 are density and density at zero pressure, respectively. Usually, the free energy is expanded to the third or fourth order in finite strain. Derivation of the free energy (truncated

to third order in finite strain) with respect to volume gives pressure and yields the third order Birch-Murnaghan EoS (e.g. Poirier 1991; Karki et al. 2001; Stixrude and Lithgow-Bertelloni 2005):

$$P = \frac{3K_{T0}}{2}\left[\left(\frac{\rho}{\rho_0}\right)^{7/3} - \left(\frac{\rho}{\rho_0}\right)^{5/3}\right]\left\{1 + \frac{3}{4}\left(K'_{T0} - 4\right)\left[\left(\frac{\rho}{\rho_0}\right)^{2/3} - 1\right]\right\} \qquad (3.9)$$

Based on the finite strain theory, an EoS for the single elastic constants can also be derived by differentiating the free energy (here truncated to fourth order in finite strain) with respect to strain (Davies 1974; Karki et al. 2001; Stixrude and Lithgow-Bertelloni 2005):

$$c_{ijkl}(f,P) = (1+2f)^{7/2}\left[c_{ijkl0} + b_1 f + 0.5 b_2 f^2 + ...\right] - P\Delta_{ijkl} \qquad (3.10)$$

$$\text{with } b_1 = 3K_{T0}\left[\frac{\partial c_{ijkl0}}{\partial P} + \Delta_{ijkl}\right] - 7c_{ijkl0} \qquad (3.11)$$

$$\text{and } b_2 = 9K_{T0}^2\frac{\partial^2 c_{ijkl0}}{\partial P^2} + 3\left(\frac{\partial K}{\partial P}\right)_{T0}\left(b_1 + 7c_{ijkl0}\right) - 16b_1 - 49c_{ijkl0} \qquad (3.12)$$

where $\Delta_{ijkl} = -\delta_{ij}\delta_{kl} - \delta_{ik}\delta_{jl} - \delta_{il}\delta_{jk}$ is -3 for longitudinal, -1 for off-diagonal and shear constants, and 0 in all other cases (e.g. Davies 1974), δ is the Kronecker delta.

3.4. Approaches to Determine Elasticity at HP/HT

The outstanding importance of knowing the H*P*-H*T* elastic behaviour of minerals for our understanding of the deep Earth has motivated a number of different experimental approaches to study both bulk and single-crystal elasticity. Aggregate elastic properties (shear and bulk modulus) can be related to one-dimensional seismic profiles (e.g. PREM) (Marquardt et al. 2009c) and are usually easier to obtain compared to single-crystal constants. However, single-crystal measurements are needed to understand seismic anisotropy observations (Marquardt et al. 2009d) and can also be used to compute aggregate elastic properties (3.2). Detailed reviews about elasticity measurements are given by Bass 2007 and Angel et al. 2009.

3.4.1. Single-Crystal Elastic Properties

Brillouin Scattering (see also experimental techniques) is the most commonly used experimental method to determine the complete elastic tensor of materials at high pressures and it has been applied to a variety of Earth materials (e.g. Weidner et al. 1982; Bass 1989; Duffy et al. 1995b; Sinogeikin and Bass 2000; Schilling et al. 2001; Speziale and Duffy 2004; Jackson et al. 2006; Marquardt et al. 2007; Marquardt et al. 2009d). Single-crystal Brillouin measurements are usually conducted at pressures up to ~20 GPa (see Polian 2003 for an overview), however, the highest pressure yet reached is 81.2 GPa (Marquardt et al. 2009c). Single-crystal Brillouin scattering has also been performed at high temperatures, both by resistive- and laser-heating (Sinogeikin and Bass 2002b; Sinogeikin et al. 2004a). Recently, first results have been reported on single-crystal Brillouin scattering experiments at simultaneously high pressure and high temperature (Sinogeikin et al. 2006; this thesis). Transparent samples (for the wavelength of the probing laser beam) are usually required for Brillouin scattering experiments, even thought it has been shown that it is, in principle, possible to probe opaque materials by surface Brillouin scattering (Crowhurst et al. 1999).

Impulsive Stimulated Light Scattering (ISLS) (Abramson et al. 1999) is another optic technique to determine the elastic tensor at high pressures. In this technique, two laser spots are used to induce counter-propagating acoustic waves that behave as acoustic grating, which is probed by a third laser. Single-crystal ISLS measurements have recently been reported on ferropericlase to 63 GPa (Crowhurst et al. 2008). ISLS can routinely be performed on optically opaque samples (Crowhurst et al. 2003; Crowhurst and Zaug 2004).

Momentum-resolved inelastic X-ray scattering (IXS) is a technique closely related to Brillouin scattering, but based on X-rays instead of visible light to probe the material (details in Burkel 2000; Burkel 2001). The shorter wavelength of x-rays compared to visible light allows access to larger segments of the dispersion curve and the sound wave velocities can be directly determined from the slope of the dispersion curve close to the Brillouin zone centre. The major advantage of using X-rays is there ability of penetrating opaque materials, such as iron or iron-alloys (Fiquet et al. 2004). Single-crystal IXS has been reported on Cobalt up to pressures of 39 GPa (Antonangeli et al. 2004a).

Gigahertz Interferometry is a method based on the creation and detection of high-frequency sound waves by piezoelectric transducers. The travel times of the sound waves through the sample are determined from the interference between waves that are reflected from both ends of the sample. The wave velocities are then calculated from the travel time

and the sample thickness. Gigahertz Interferometry was used to measure single-crystal elastic properties of a variety of compounds at pressures below 10 GPa and relatively low temperatures (Reichmann et al. 2000; Jacobsen et al. 2002; Jacobsen et al. 2004) and can be used to study optically opaque materials.

Computational (ab-initio) approaches have also been used to compute the elastic tensor of Earth materials at high pressure and high temperature (Karki et al. 1997; Karki et al. 1999; Karki et al. 2001; Stackhouse et al. 2005; Stackhouse et al. 2006; Wentzcovitch et al. 2006), but are mostly limited to iron free endmember compositions, due to difficulties in describing transition metals and large assemblies. However, computational methods are evolving rapidly and first successful attempts to describe iron containing systems, using extended density functional theory calculations (DFT+U), have been reported (Persson et al. 2006; Tsuchiya et al. 2006b; Da Silva et al. 2008; Umemoto et al. 2008).

3.4.2. Elastic Properties of Aggregates

Brillouin scattering was also used to measure bulk elastic properties on polycrystalline materials (Sinogeikin and Bass 2002a; Murakami et al. 2007a; Murakami et al. 2007b; Murakami et al. 2009), allowing for higher pressures (up to 172 GPa) than single-crystal measurements. Recently, first attempts have been reported to perform Brillouin scattering experiments on polycrystalline MgO at simultaneously high pressure and high temperature (Murakami et al. 2008). However, the use of polycrystalline materials might cause significant problems, which have not yet been adequately adressed (see chapter 4.3.2).

Impulsive Stimulated Light Scattering (ISLS) has also been used with polycrystalline samples to pressures above 100 GPa (e.g. Goncharov et al. 2004; Crowhurst et al. 2005).

Momentum-resolved inelastic X-ray scattering (IXS) has been reported on polycrystalline materials to pressures up to ~110 GPa (Fiquet et al. 2001; Antonangeli et al. 2004b) and also at moderately high temperatures (Kantor et al. 2007).

Shock waves can be used to constrain sound wave velocities at extreme pressures and temperatures (several hundred GPa and thousands of K), which are inaccessible by all other methods. In a shock wave experiment, a flyer plate hits a target material and produces a region of compression, which then propagates through the sample material at supersonic velocity. Among other physical properties, sound wave velocities can be extracted from shock

wave experiments (e.g. Brown and McQueen 1986; Duffy and Ahrens 1995; Nguyen and Holmes 2004).

Ultrasonic methods in High-Pressure Devices are based on the direct creation and detection of sound waves in a sample via ultrasonic transducers (details in Bass 2007). The sample is placed in a high-pressure device, such as a piston-cylinder apparatus for relatively low pressures (e.g. Jackson et al. 1981; Jackson et al. 1990; Mueller et al. 2002) or a Multi-Anvil Device for higher pressures and high temperatures (e.g. Mueller et al. 2002; Mueller et al. 2005; Bass 2007). Ultrasonic measurements in Multi Anvil Devices have been reported at pressures and temperatures corresponding to Earth's transition zone (Higo et al. 2008).

Nuclear Resonant Inelastic X-ray Scattering (NRIXS) (Sturhahn 2004) allows to determine the phonon density of states (PDOS) by the response of a nucleus to excitation by X-rays at a specific resonant energy. A nuclear resonant isotope, such as ^{57}Fe, is therefore required in NRIXS experiments. Theoretical assumptions, i.e. the Debye model, have to be applied to determine aggregate sound wave velocities from the measured PDOS (Hu et al. 2003). NRIXS has been reported to pressures corresponding to the Earth's core (Mao et al. 2001; Lin et al. 2006) and also to simultaneously high temperatures (Lin et al. 2005b). However, it appears that there are still unsolved problems in the interpretation of the obtained data at least for some iron containing compounds (McCammon et al. 2008b), which are possibly caused by only probing a partial PDOS related to the resonant isotope.

X-ray diffraction data at high pressures can be used to extract the isothermal bulk modulus $K_T = -V \cdot \mathrm{d}P/\mathrm{d}V$ from the $P(V)$ data and it has been measured to extremely high pressures (Mao et al. 1989) and temperatures (Dubrovinsky et al. 2007). No accurate information about shear properties can be derived.

Brillouin scattering in conjunction with x-ray diffraction was the technique of choice for the purpose of this thesis as it is capable of determining the complete elastic tensor, including the shear constants, with high accuracy up to the high pressures of Earth's lower mantle.

4. Methods

4.1. Diamond-Anvil Cell (DAC)

To date, diamond-anvil cells (DAC) are the only pressure devices that are capable of generating static pressures corresponding to Earth's lower mantle and core (Mao et al. 1989; Mao et al. 1990). In a DAC (fig. 4.1), static pressure is applied to a small sample (e.g. ~50 µm diameter, ~20 µm thickness) via two opposing diamond anvils with their tips (culets) pointing towards each other and the sample sandwiched in between (e.g. Jayaraman 1983). The applied force F is converged to a very small area a, allowing for extremely high pressures P (>300 GPa) with a moderate force because $P = F/a$. A metal ring (gasket), often made of stainless steel, rhenium, or beryllium, is used to keep the pressure within the sample chamber.

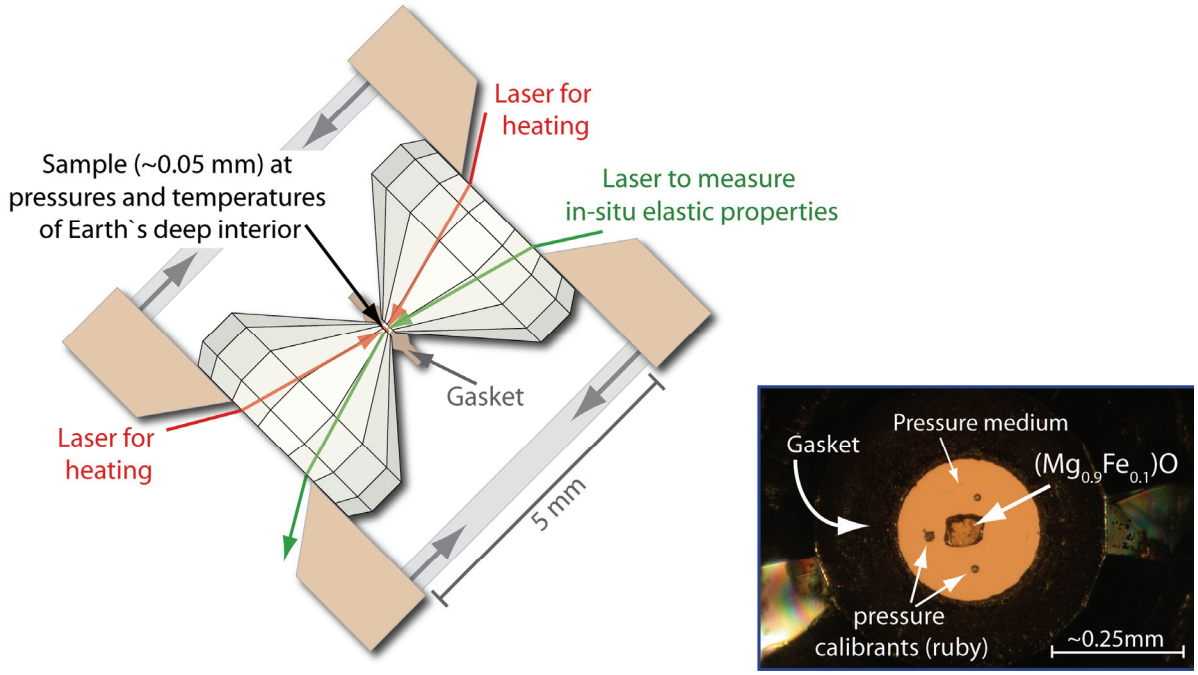

Fig. 4.1: Working principle of a diamond-anvil cell with illustration of laser heating and Brillouin scattering. Very high pressures are generated by applying a moderate force on a very small area. The photo on the right shows a view through one diamond anvil into the sample chamber. The sample chamber is loaded with neon, which serves as pressure-transmitting medium.

A pressure-transmitting medium is employed to convert the applied uniaxial stress to a quasi-hydrostatic pressure. The most commonly used pressure-transmitting media in cold compression experiments are a methanol-ethanol(-water)-mixture, argon, neon, or helium.

Recent single-crystal x-ray diffraction results suggest that argon already supports considerable shear stresses at low pressures, which is indicative of a low hydrostatic limit (Angel et al. 2007). It is widely accepted that neon and helium are today's best pressure-transmitting media (e.g. Kenichi 2001 and references therein), but relatively few experiments are carried out using these media, due to the experimental difficultes in loading them into the DAC (Kurnosov et al. 2008). Neon and helium must be loaded as gases under high pressure (~2 kbar). All pressure-transmitting media are solid under pressures corresponding to the lower mantle, neon for instance, crystallizes at 4.6 GPa (at 300 K) (Shimizu et al. 2005).

Different methods can be used to monitor pressure in the DAC. Most commonly, ruby is used as a pressure calibrant. The shift of the ruby fluorescence line R_1 is measured (fig. 4.2) and related to pressure, where different calibrations can be used (e.g. Mao et al. 1978; Mao et al. 1986; Zha et al. 2000; Holzapfel 2003; Dorogokupets and Oganov 2007). When performing x-ray diffraction experiments at high-pressures, it is also possible to load a reference material, such as gold, with known Equation of State and compute pressure from the measured unit cell volume (e.g. Fei et al. 2007a). Diamond anvil cells can be used in combination with a large number of experimental techniques to determine various physical properties in-situ, a detailed review is given by Mao and Mao 2007.

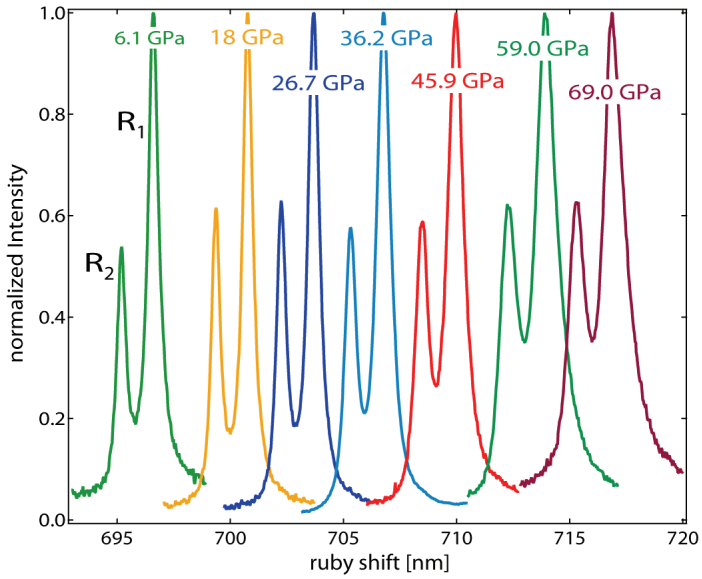

Fig. 4.2: Ruby fluorescence spectra at different pressures in neon pressure-transmitting medium. A slight broadening of the ruby lines is observable with increasing pressure, which can be related to non-hydrostatic pressures in the sample chamber. The shift of the ruby R_1 line is used to calculate pressure by using the ruby pressure calibration of Mao et al. 1986.

4.1.1. High-temperature DAC

In addition to pressure, high temperatures can be realized in the DAC by either external resistance or internal laser heating (Boehler 1992; Boehler 2000).

When using an external resistance heating system, the sample chamber is homogenously heated, but temperatures are limited to about 800°C. An externally heated DAC as used in this thesis (chapter 5.3) to perform Brillouin scattering at simultaneously high-pressures and high-temperatures at the Advanced Photon Source is shown in figure 4.3. In this setup, $Pt_{90}Rh_{10}$ alloy served as heating wire and both type K (Ni/NiCr) and S (Pt/PtRh) thermocouples were used to monitor temperature and control a temperature feedback system to maintain a constant temperature for several hours.

Laser (e.g. YLF, CO_2) heating allows for much higher temperatures (several thousands of Kelvin), but creates an enormous temperature gradient, some thousands of degrees within a tenth of a millimetre, in the sample chamber (Boehler 2000). The temperature is measured by analysing the thermal radiation emitted from the sample according to Planck's radiation function (Boehler 2000).

Simulating the *P*-*T*-conditions of Earth's lower mantle (Dubrovinsky et al. 2000; Murakami et al. 2004) and core (Dubrovinsky et al. 2007) in the DAC is experimentally possible. However, a precise determination of pressure and especially temperature at these conditions is very difficult (e.g. Irifune et al. 2005). When using a heated DAC, the choice of pressure-transmitting medium is less critical due to temperature-induced stress annealing.

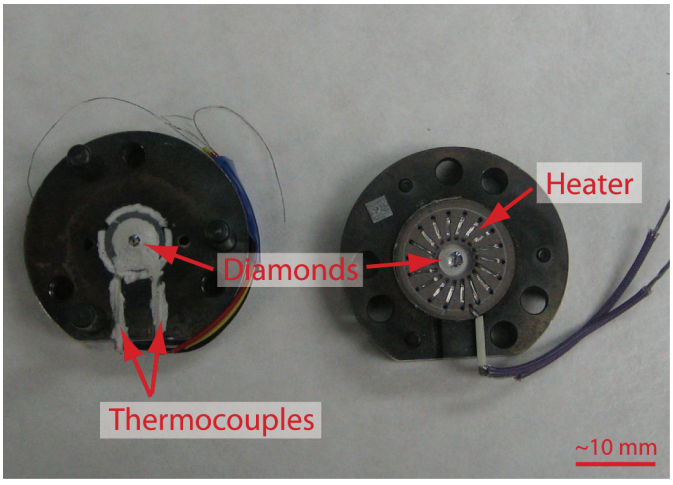

Fig. 4.3: Setup of an externally heated diamond anvil cell (S. Sinogeikin's design) as it is used to conduct Brillouin scattering at combined high-pressure and high-temperature at Sector 13 of the Advanced Photon Source.

4.2. Brillouin Scattering

4.2.1. Introduction

In any given material at a temperature >0 K, atoms are in thermal motion and oscillate around their equilibrium positions. The particle displacements are coupled and correspond to travelling (or standing) waves (phonons), which introduce local periodic perturbations of the dielectric constant. These periodic differences in optical density elastically scatter light following Bragg's Law (in the classical picture). In the case of sound waves (acoustic phonons), the periodic perturbations travel with the speed of sound, which causes inelastic scattering contributions according to the Doppler effect that depend on the acoustic velocities (a quantum mechanical equivalent is shown in fig. 4.4). In Brillouin scattering experiments, the resulting frequency shift of the probing laser light is analysed and related to the propagation speed of the acoustic phonons. A theoretical prediction of this phenomenon was presented in the 1920s (Brillouin 1922; Mandelstam 1926), the first experimental observation was reported in 1930 (Gross 1930). Detailed reviews of Brillouin scattering are given by e.g. Cummins and Schoen 1972; Grimsditch 2001.

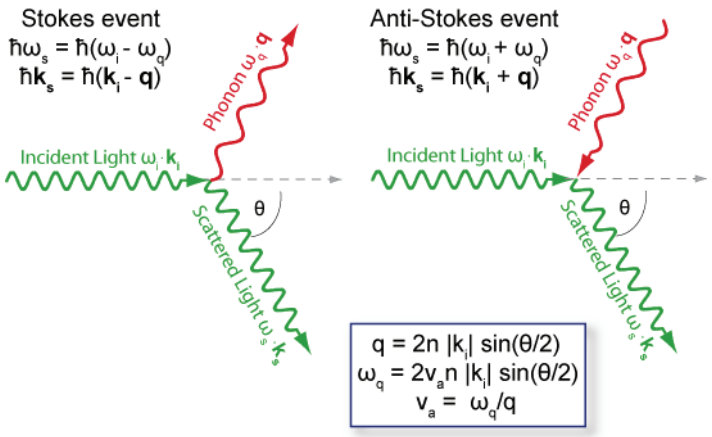

Fig. 4.4: Quantum mechanical picture of the Brillouin scattering process. The incident laser light is inelastically scattered by acoustic phonons in the sample where a phonon is either created (Stokes event) or annihilated (Anti-Stokes event). Conservation of energy ($\hbar\omega$) and momentum ($\hbar\boldsymbol{k}$) is required. The acoustic velocity v_a can be calculated from the difference in frequency between incident and scattered light. Symbols in the figure are Planck's constant $\hbar$, angular frequency ω, wave vector of incident and scattered light $\boldsymbol{k_i}$ and $\boldsymbol{k_s}$, phonon wave vector $\boldsymbol{q}$ and refractive index n.

4.2.2. Experimental Setup

Brillouin scattering experiments are often carried out in symmetric platelet forward scattering geometry (fig. 4.5), where - in an optically isotropic medium and with the assumption that the wavelength of incident and scattered light are equal - the relation between measured frequency shift ν and interacting phonon velocity V is given by (Whitfield et al. 1976):

$$V = \frac{\nu \cdot \lambda_0}{2 \cdot \sin \frac{\sigma_{ext}}{2}} \qquad (4.1)$$

where σ_{ext} is the external scattering angle and λ_0 is the wavelength of the laser (in air). Brillouin scattering experiments at ambient pressure are commonly carried out with an external scattering angle of 90°, whereas high-pressure experiments demand smaller scattering angles (e.g. 60°) due to the limited optical access to the DAC. The wave vector of the scattering phonon is parallel to the platelet surface (fig. 4.5) and a rotation of the sample allows for probing different phonon directions. If the density of the material is known, the measured velocities can be inverted for the elastic constants via the Christoffel equation (Every 1980, see also chapter 3.1). Brillouin scattering of materials of high symmetry also allows to determine the crystallographic orientation of the sample with high accuracy (e.g. Every 1980; Duffy et al. 1995b; Sinogeikin and Bass 2000; Speziale and Duffy 2004).

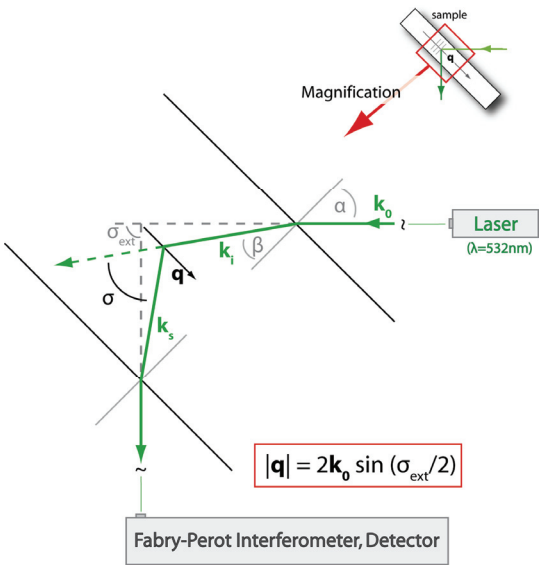

Fig. 4.5: Symmetric platelet scattering geometry (θ_{ext} = 90°). $\boldsymbol{k_i}$ is the wave vector of the incident laser (out of the sample). $\boldsymbol{k_i}$ and $\boldsymbol{k_s}$ refer to the wave vectors of the incident and scattered light in the sample, $\boldsymbol{q}$ refers to the scattering phonon wave vector. In the special case of symmetric platelet scattering geometry, knowledge of the refractive index is not required to relate the measured frequency shifts to the acoustic velocities (e.g. Whitfield et al. 1976; Sinogeikin and Bass 2000).

The Brillouin system at Deutsches GeoForschungsZentrum Potsdam is shown in figure 4.6. It consists of a Nd:YVO_4 solid state laser, operating at a wavelength (λ_0) of 532 nm, as light source and a Sandercock-type tandem six-pass Fabry-Perot (FP) interferometer (Sandercock 1982) equipped with a photomultiplier tube for signal detection (Speziale et al. 2007b).

The vast majority of light that is scattered towards the Interferometer did not exchange energy with the acoustic phonons and thus the peaks corresponding to the inelastically scattered component of the analysed light are very weak compared to the peak corresponding to the elastic scattering events (Rayleigh peak). In addition, the Brillouin frequency shifts are very small (in the order of 1 cm^{-1}). The close proximity of the Brillouin peaks to the elastic peak, combined with the enormous contrast in amplitude, requires the use of an interferometer with very high resolution and contrast. Usually, a Sandercock-type tandem multipass Fabry-Perot interferometer (Sandercock 1982) is used. Two parallel semireflecting plane mirrors are used in a FP interferometer and their distance is periodically scanned over a distance roughly corresponding to the wavelength of the incident laser light, so that constructive interference and thus transmission only occurs for a specific wavelength at any time. In a tandem FP interferometer, two pairs of mirrors are installed in series and their distance is slightly different to suppress higher orders of the interference pattern. In a tandem multipass FP interferometer, the scattered laser light is guided a number of times through the pairs of mirrors (six times in the FP at GFZ Potsdam).

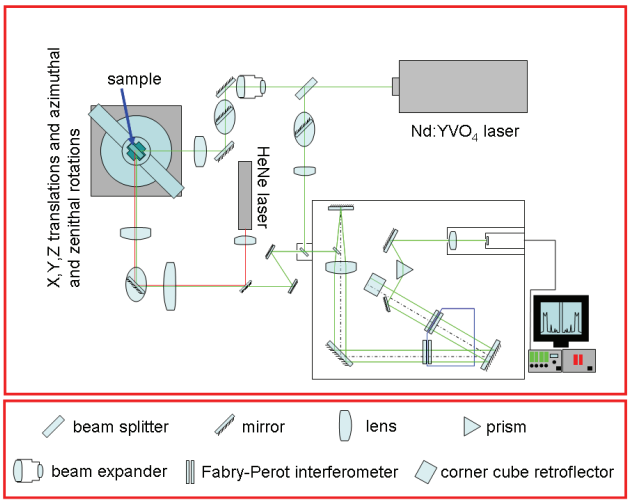

Fig. 4.6: Brillouin system at GFZ Potsdam (courtesy of Sergio Speziale). A green Nd:YVO_4 solid state laser serves as light source. The monochromatic light (λ = 532nm) is focused on the sample, which is mounted to a goniometer. The scattered light is analysed for frequency in a six-pass tandem FP interferometer. Turning of the sample in the goniometer allows to probe different phonon directions. The red HeNe laser is needed as a reference to calibrate sample position and scattering geometry.

4.2.3. Brillouin Scattering in Earth Sciences

Brillouin spectroscopy is a widely used technique to determine the elastic tensor of both natural and synthetic Earth materials. It has been applied to a number of relevant crystalline solids, glasses, and liquids. Most commonly, Brillouin scattering is performed on single-crystals where the outcome is the complete elastic tensor of the sample material (e.g. Duffy et al. 1995b). Because Brillouin scattering is an optical method, it can be carried out at high-pressures (and also high-temperatures) in a diamond-anvil cell. One major drawback of Brillouin scattering experiments is the need for transparent, or at least semitransparent, samples in order to determine body wave velocities. Previous studies of mantle phases, which are typically solid solution series between Mg- and Fe-endmember, have therefore been limited to compositions very close to the Mg-endmember (e.g. Zha et al. 2000; Jackson et al. 2004; Jackson et al. 2006). However, contrary to what has been reported earlier (Mao and Bell 1972), it turned out in the past few years that the major components of the Earth's mantle $(Mg,Fe)_2SiO_4$, $(Mg,Fe)SiO_3$ and (Mg,Fe)O remain transparent in their stability field, even when they contain realistic amounts of iron (~10 at.%) (Keppler and Smyth 2005; Keppler et al. 2007; Keppler et al. 2008). These new findings further emphasize the importance of Brillouin scattering for high-pressure (and high-temperature) research in Earth sciences.

Brillouin scattering of polycrystalline materials

Brillouin scattering has also been measured from polycrystalline materials. A good agreement for bulk properties (shear and bulk modulus) between Brillouin scattering measurements performed on polycrystalline and single-crystal perovskite has been demonstrated at ambient conditions (Sinogeikin et al. 2004b). Hence, Brillouin scattering on polycrystalline materials promises to be an easy and direct way to obtain aggregate (bulk and shear) moduli of candidate minerals which can be related to seismological observables.

Recently, Brillouin experiments on polycrystals have been performed to very high pressures (Murakami et al. 2007a; Murakami et al. 2007b; Murakami et al. 2009). However, the quality and reliability of bulk properties determined by Brillouin scattering on polycrystalline materials at high pressures is not completely understood. As the stress distribution in a diamond-anvil cell at high pressures will not be uniform, a major complication might arise from the development of a lattice-preferred orientation (LPO) in the polycrystalline sample that would no longer represent an isotropic aggregate. In this case, the measured aggregate velocity will be an average weighted by the grains' orientation

distribution function and could strongly deviate from the isotropic average velocity. Furthermore, the anisotropic deformation behaviour of the constituents leads to intergranular stresses, which may bias the measured velocity.

Brillouin scattering at high-pressure

Being an optical, contact-free method, Brillouin scattering measurements can be conducted on samples that are pressurized in a diamond-anvil cell (Whitfield et al. 1976). Figure 4.7 shows a diamond-anvil cell containing $(Mg_{0.9}Fe_{0.1})O$ at a pressure of 81.2 GPa mounted to the Brillouin System at GFZ Potsdam. A detailed analysis of possible sources of errors and difficulties when performing Brillouin scattering in a DAC is given in Zha et al. 1996 and Sinogeikin and Bass 2000. Due to experimental complexity, most studies have been limited to pressures of the upper mantle below ~25 GPa (e.g. Duffy et al. 1995b; Zha et al. 1996; Zha et al. 1997; Sinogeikin and Bass 2000; Sinogeikin and Bass 2002a; Sinogeikin et al. 2003; Speziale and Duffy 2004; Speziale et al. 2006; Jackson et al. 2006; Wang et al. 2006; Reichmann et al. 2008), and only very few studies have reached pressures corresponding to the lower mantle (Zha et al. 1998; Zha et al. 2000; Murakami et al. 2007b; Murakami et al. 2009). To date, the maximum pressure reached in single-crystal Brillouin studies is 81.2 GPa (Marquardt et al. 2009c), measurements of polycrystalline samples achieved 172 GPa (Murakami et al. 2007a).

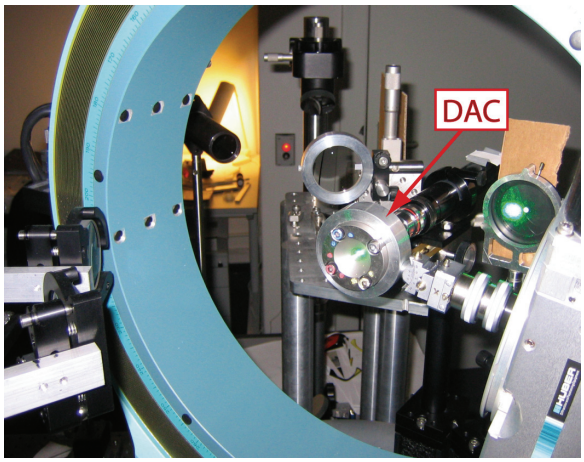

Fig. 4.7: Goniometer with DAC for high-pressure Brillouin scattering experiments. The sample in the DAC is at a static pressure of 81.2 GPa. Brillouin scattering measurements in different phonon directions, i.e. azimuthal angles within the goniometer, facilitate the determination of the elastic tensor along with the sample orientation.

Brillouin scattering at high-temperature

Both external heating (Askarpour et al. 1993; Sinogeikin et al. 2000; Jackson et al. 2000; Sinogeikin and Bass 2002b; Sinogeikin et al. 2003; Jackson et al. 2007) and laser heating

systems (Sinogeikin et al. 2004a) have been successfully employed to perform Brillouin scattering experiments at high-temperature and ambient pressure.

Brillouin scattering at simultaneously high-pressure and high-temperature

First results on successful single-crystal Brillouin scattering in an externally heated DAC at simultaneously high-pressure (30 GPa) and high-temperature (500 °C) (Sinogeikin et al. 2006; Sinogeikin et al. 2007) have been published. As part of this thesis, Brillouin scattering experiments of ferropericlase were performed in an externally heated DAC (chapter 4.1.1). Very recently, Murakami et al. 2008 reported first preliminary Brillouin scattering results on the elasticity of polycrystalline MgO at 49 GPa and 2000 °C laser-heated in a DAC.

4.3. X-ray Diffraction

In any x-ray diffraction experiment (fig. 4.8), x-ray photons with wavelength λ are elastically scattered by a set of lattice planes with spacing d_{hkl}, while trespassing a sample material following Bragg's law:

$$\lambda = 2 \cdot d_{hkl} \cdot \sin(\theta) \qquad (4.2)$$

where 2θ is the scattering angle. If the wavelength of the incident x-ray photons is known and the diffraction angle is measured, the *d*-spacing can be determined. The *d*-spacings are related to the lattice parameters and the unit-cell volume of the probed material.

Both single-crystals and powders are studied by x-ray diffraction. The use of powders has the advantage that several different lattice planes simultaneously satisfy Bragg's Law at a given scattering angle. This is a reason why powders are usually preferred for high-pressure experiments in the diamond anvil cell, where the angular access to the sample is very limited, because the diamond seats are usually not x-ray transparent (fig. 4.8).

4.3.1. Synchrotron X-ray Powder diffraction at H*P*

X-ray powder diffraction at high-pressures in the diamond anvil cell is a standard technique to put constraints on phase stability fields and determine equations of state of materials (e.g. Mao et al. 1989; Duffy et al. 1995a). Because the space for sample material in the pressure chamber is very limited, there is need for high-intensity radiation to obtain diffraction data in reasonable time. Therefore, high-pressure x-ray powder diffraction studies are usually carried out at synchrotron sources. Powder diffraction experiments at H*P* have been conducted as part of this thesis at the Diamond Light Source in the UK (Marquardt et al. 2009c; Marquardt et al. 2009d).

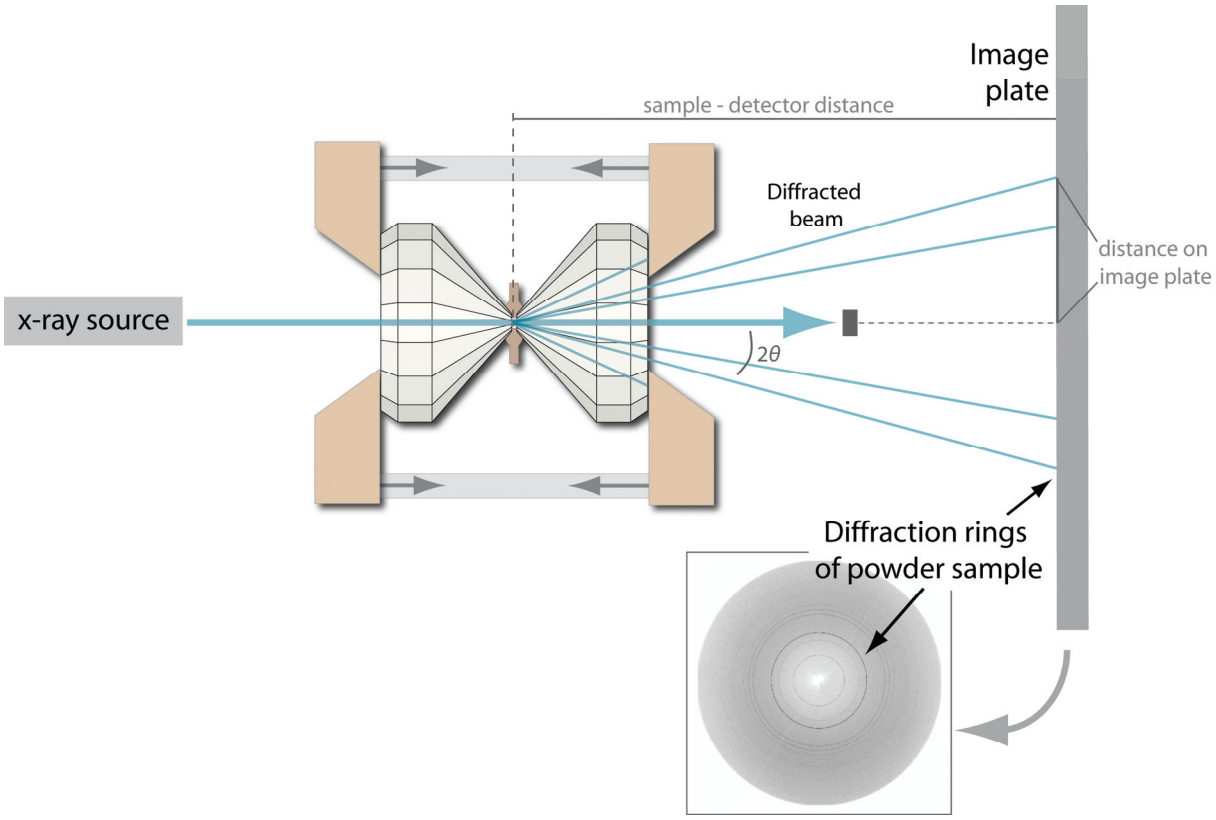

Fig. 4.8: Illustration of the experimental setup for angle-dispersive high-pressure powder x-ray diffraction in a diamond-anvil cell. A monochromatic x-ray beam is focused in the sample, which is loaded in a diamond-anvil cell. A part of the incident radiation is elastically scattered following Bragg's law. The scattering angles 2θ can be determined from the collected diffraction rings, if the distance between sample and image plate is known. According to eq. 4.2, the scattering angles and corresponding *d*-spacings are related by the wavelength of the probing beam.

4.3.2. Single-Crystal Synchrotron X-ray Diffraction at H*P*/H*T* in Combination with Brillouin Scattering

The experimental setup at Sector 13 (GSECARS) of the Advanced Photon Source (APS) allows for simultaneously measuring x-ray diffraction and Brillouin scattering. The capability of collecting sound velocity and density in parallel makes it possible to derive the elastic constants even if the density of the material can not be obtained from the Brillouin data. An example is the density of ferropericlase across the spin transition in Fe^{2+} (Marquardt et al. 2009c; Marquardt et al. 2009d). Additionally, the phonon direction selected for Brillouin scattering can be determined from the x-ray diffraction pattern, which, in principle, allows for reducing the number of measurements that are required to determine the elastic tensor to very few phonon directions - one direction can be sufficient for materials with cubic symmetry. A combined measurement of x-ray diffraction and sound wave velocities also has the potential to set up an independent pressure scale (e.g. Zha et al. 2000; Mueller et al. 2003; Sinogeikin et al. 2007).

However, to date there are only two laboratories around the world (APS in USA, SPring-8 in Japan) where Brillouin scattering and X-ray diffraction can be performed at the same time (Sinogeikin et al. 2006; Murakami et al. 2008). As part of this thesis, Brillouin scattering and x-ray diffraction were conducted simultaneously on ferropericlase at high-pressure and high-temperature at the APS (chapter 5.1.3).

4.4. Multi Anvil Device

Multi anvil presses (detailed review in Ito 2007) are also called large volume presses, because they allow to load significantly larger samples (up to 2 cm^3) (Frost et al. 2004) than it is possible in DACs. To date, the maximum *P*-*T*-conditions that can be achieved in a multi anvil press are corresponding to the upper part of the lower mantle. However, the use of sintered diamond anvils (instead of commonly used WC) allows for higher pressures ~60 GPa (Utsumi et al. 1986; Ito 2006; Tange et al. 2009) and promises to achieve even higher pressures (Ito et al. 2008). Multi anvil presses can be used to synthesise material at certain *P*-*T*-conditions, either to study phase-equilibria (e.g. Katsura and Ito 1989) or to produce samples that are then studied using other techniques (e.g. Marquardt et al. 2009c; Marquardt et al. 2009d). Several

techniques (such as ultrasonic interferometry, electrical conductivity measurements, or x-ray diffraction) for in-situ studies of physical properties can be combined with large volume presses (e.g. Yagi and Akimoto 1976; Katsura et al. 1998; Katsura et al. 2004; Ito 2007; Higo et al. 2008). The ferropericlase samples that were studied for this thesis were grown in a multi-anvil apparatus at the Bayerisches Geoinstitut at *P*-*T*-conditions corresponding to the uppermost regions of Earth's lower mantle (details in Marquardt et al. 2009d).

5. Results and Discussion – Extended Abstracts

This chapter summarizes the results that emerged from my PhD-research. The outcomes are presented in the following chapters 5.1 to 5.. The three major parts of this thesis (chapter 5.1, 5.2, and 5.4) are published or submitted for publication in international scientific journals and are summarized here. The complete manuscripts, including supplementary materials, can be found in chapter 6.

5.1. Single-Crystal Elastic Properties of Ferropericlase to 81 GPa

(This abstract is based on the following article: Marquardt, H., S. Speziale, H. J. Reichmann, D. J. Frost and F. R. Schilling (2009). Single-Crystal Elastic Properties of $(Mg_{0.9}Fe_{0.1})O$ to 81 GPa. *Earth Planet. Sci. Lett.* **submitted**.)

To date, the most complete picture of the structure, evolution and present-day dynamics of the Earth's lower mantle emerges from seismological observations. An interpretation of seismic wave velocities in terms of mineralogy and temperature requires detailed knowledge of the physical properties of candidate phases at *PT*-conditions relevant to the Earth's deep interior.

In this paper, the elastic properties of $(Mg_{0.9}Fe_{0.1})O$ ferropericlase, presumably the second most abundant mineral in the lower mantle (e.g. Bina et al. 2003), are presented. The elastic behaviour was studied by Brillouin scattering and x-ray diffraction in a diamond-anvil cell to 81 GPa. The HS-LS transition has sensitive effects on the longitudinal and off-diagonal elastic stiffness constants, but does not clearly affect the shear constants. This mechanism leads to a considerable "softening" of the compressional and bulk velocity but does not lower shear wave velocities (fig. 5.1). At high temperatures, the decrease in v_p will likely spread over a large depth range, which would result in a decreased v_p/v_s ratio throughout most or all of the lower mantle.

The HS-LS transition strongly affects the temperature derivative of the longitudinal and bulk velocities at pressures where the elastic behaviour is influenced by the spin transition. At specific pressure-temperature combinations (relevant for the mid-lower mantle), the spin transition can also lead to an anti-correlated temperature dependence of shear and compressional (and bulk) velocity, where a lower temperature will be accompanied by higher

shear velocities, but decreased longitudinal and bulk velocities. Based on our modelling, this mechanism is expected to occur only in some parts of the lower mantle between roughly 1300 and 1800 km depth.

Seismologists have not yet reported clear evidences of effects directly caused by the ocurrence of the spin transition in the lower mantle. This might be due to the broad depth interval over which the spin transition likely occurs at *P-T*-conditions of the deep Earth and the resulting absence of seismic wave reflections, combined with the minor volume contribution of ferropericlase in a typical lower mantle assemblage (~20 Vol.%), which masks its anomalous elastic behaviour across the transition.

The broadness and magnitude of the perturbation in velocity ratios associated with the transition change with both temperature and iron-content. However, our current knowledge indicates that the variation with temperature and composition is different, where temperature broadens the spin transition (Sturhahn et al. 2005; Tsuchiya et al. 2006b; Lin et al. 2007) and iron increases the magnitude of perturbation (Lin and Tsuchiya 2008, this study). Increasing the iron content eventually also broadens and pressure-shifts (Speziale et al. 2005; Persson et al. 2006) the transition, but possibly not significantly for iron contents below ~25 at.% (Speziale et al. 2007a). If these mechanisms are well understood and if specially designed future seismological studies succeed to resolve its elastic signature, the spin transition could provide important constraints on both temperature and iron distribution in Earth's mid-lower mantle.

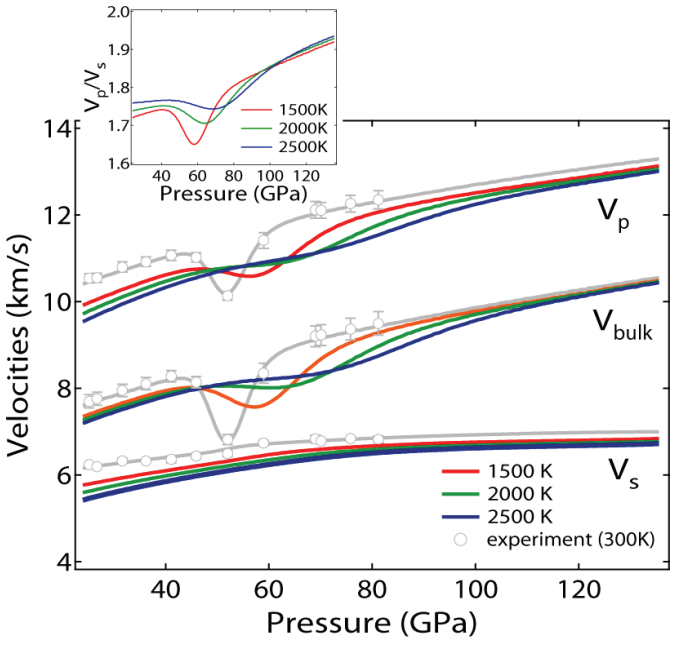

Fig. 5.1: Average velocities as a function of pressure and temperature. The bulk velocity $v_{bulk} = (K_s/\rho)^{0.5}$ is strongly affected by the spin transition due to its close relation to the bulk modulus. Also the longitudinal wave velocity is significantly lowered, even though they depend on both bulk and shear modulus ($v_p = [(K_s+4/3G)/\rho]^{0.5}$). Almost no change is observable for the shear wave velocity. The spin transition of Fe^{2+} in ferropericlase might cause an anti-correlated temperature dependence of p- and s-wave velocities. A temperature decrease of 500 K at a pressure of 60 GPa could, for instance, decrease p-wave velocities of $(Mg_{0.9}Fe_{0.1})O$ by 1.3% (bulk velocities would even be decreased by 4%) and at the same time increase s-wave velocity by 1.8%.

The inset shows the ratio of compressional and shear wave velocities, which is markedly depressed by the HS-LS transition. The temperature effect was modelled using the thermoelastic parameters reported for MgO (Karki et al. 1999) and estimating the change of spin transition pressure region with temperature from a computational study (Tsuchiya et al. 2006a).

5.2. Elastic Shear Anisotropy of Ferropericlase in Earth's Lower Mantle

(This abstract is based on the following article: Marquardt, H., S. Speziale, H. J. Reichmann, D. J. Frost, F. R. Schilling and E. J. Garnero (2009). Elastic Shear Anisotropy of Ferropericlase in Earth's Lower Mantle. *Science* **324**(5924): 224-226.)

Seismic shear anisotropy is a key feature within many regions of the lowermost mantle (the D'' layer) (Kendall and Silver 1996; Lay et al. 1998; McNamara et al. 2002; Garnero et al. 2004; Panning and Romanowicz 2004; Wookey et al. 2005), which likely results from lattice preferred orientation (LPO) caused by plastic deformation coupled with strong elastic anisotropy of lower mantle minerals (Karki et al. 1999; McNamara et al. 2002; Yamazaki and Karato 2002; Wookey et al. 2005; Wenk et al. 2006). An understanding of the mineral properties and their deformation behaviour that lead to seismic anisotropy can provide important information on mantle flow in these regions (McNamara et al. 2002; Panning and Romanowicz 2004; Wookey et al. 2005). Even though (Mg,Fe)O ferropericlase constitutes only ~20 Vol.% of the lower mantle, it is supposed to contribute significantly to the observed seismic shear anisotropy (McNamara et al. 2002; Yamazaki and Karato 2002; Wenk et al. 2006). The elastic shear anisotropy of ferropericlase in the lower mantle, however, remains largely unknown, especially across the spin transition of iron, restricting the interpretation of seismic shear anisotropy observations in terms of evolution and dynamics of Earth's lower mantle (Yamazaki and Karato 2002; Wenk et al. 2006).

In this study, the elastic shear anisotropy of single-crystal $(Mg_{0.9}Fe_{0.1})O$, a composition likely close to a typical lower mantle ferropericlase, is presented up to 69 GPa measured by Brillouin scattering in a diamond anvil cell. The results show that the elastic shear anisotropy of (Mg,Fe)O increases significantly across the pressure-induced spin transition of iron (Badro et al. 2003) between 40 and 60 GPa, the increase of iron content further enhances the anisotropy. The effect of the spin transition, together with the effect of Fe-Mg substitution, leads to at least 50% stronger elastic shear anisotropy of (Mg,Fe)O at the base of the lower mantle than reported for MgO (Karki et al. 1999), which was previously

used for geodynamic modelling (Yamazaki and Karato 2002; Wenk et al. 2006). The contribution of the unexpected high elastic shear anisotropy of ferropericlase to the maximum potential aggregate anisotropy of a typical lower mantle assemblage rivals that of the more abundant silicate perovskite or post-perovskite (fig. 5.2). As ferropericlase is rheologically weaker (Karato 1989) than silicate minerals it will be the dominant cause of seismic shear anisotropy in the lower mantle (Kendall and Silver 1996; Lay et al. 1998; McNamara et al. 2002; Garnero et al. 2004; Panning and Romanowicz 2004; Wookey et al. 2005).

The picture emerging from these new results is that ferropericlase is probably dominating the elastic anisotropy of the lower mantle in all the environments where the deformation of mantle rock takes place by dislocation creep, which favours the development of lattice preferred orientation, and the strain level is elevated (McNamara et al. 2002). The apparent absence of seismic anisotropy in large sectors of the lower mantle (as put forth in Panning and Romanowicz 2006) might suggest that the bulk lower mantle is dominated by conditions at which deformation is controlled by diffusion creep that does not enhance lattice preferred orientation (Karato et al. 1995; Yamazaki and Karato 2001).

However, there are large uncertainties on the depth distribution of seismic anisotropy in the deep lower mantle (Wenk et al. 2006) and even if the lower mantle above D" is moderately (or even strongly) anisotropic, and if the mixing and convection scales in the lower mantle are such that the anisotropy signatures are not uniform over significant lateral scales, it is possible that seismic waves cannot properly depict the anisotropy, and it is instead mapped as isotropy.

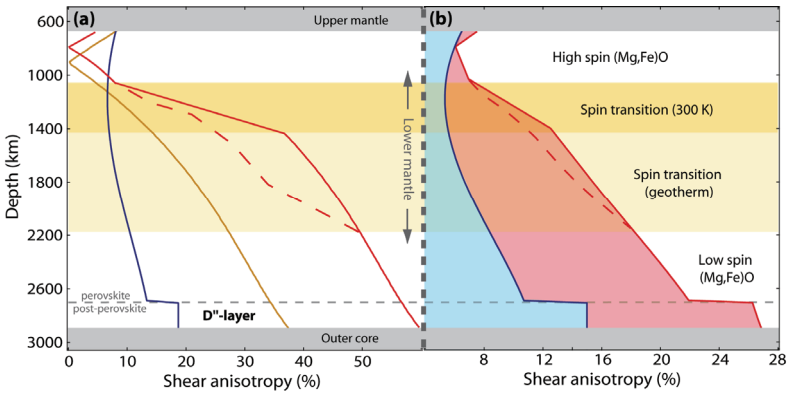

Fig. 5.2: Maximum shear anisotropy of major lower mantle phases and MgO for comparison along a model geotherm (Stacey 1992). The shear polarization anisotropy is defined as $(v_{s,max}-v_{s,min})/((v_{s,max}+v_{s,min})/2)$, where $v_{s,max}$ and $v_{s,min}$ are maximum and minimum shear velocity in a given direction. (a) shows the maximum single-crystal polarization anisotropy of the two major components of Earth's lower mantle. The shear anisotropy of MgO (gold) and $MgSiO_3$ (blue) were calculated using

available computational data at high pressure and temperature (Karki et al. 1999; Wentzcovitch et al. 2004). The elastic anisotropy of $(Mg_{0.8}Fe_{0.2})O$ (red), a model mantle composition, was linearly scaled from the data of MgO (Karki et al. 1999) and $(Mg_{0.9}Fe_{0.1})O$, corrected for temperature effects. The expected broadening of the spin transition region (dashed lines) with temperature was estimated from experimental data on $(Mg_{0.75}Fe_{0.25})O$ (Lin et al. 2007). (b) The anisotropies of the single phases were weighted by their volume abundance in the lower mantle (Lee et al. 2004), where the shaded areas illustrate the maximum possible contributions of perovskite (blue) and ferropericlase (red), a situation where all the crystals of the same mineral phase have the same orientation. As (Mg,Fe)O is a much weaker phase (Karato 1989), it will accommodate most of the strain (Madi et al. 2005); it should, therefore, develop a much stronger texture than $(Mg,Fe)SiO_3$ (Wentzcovitch et al. 2006).

5.3. Effect of Temperature on the Single-Crystal Elasticity of Ferropericlase

(article in preparation)

Elastic properties do not only change with pressures but also with temperature, even though the pressure-effect is usually more pronounced along a geotherm in Earth's interior. In Marquardt et al. 2009c and Marquardt et al. 2009d, the effect of temperature on elasticity is modelled based on available computational data for MgO (Karki et al. 1999). To place experimental constraints on the temperature dependence of elastic properties in (Mg,Fe)O, Brillouin scattering experiments on single-crystal ferropericlase $(Mg_{0.9}Fe_{0.1})O$ were performed at combined high-pressures and high-temperatures at Sector 13 of the Advanced Photon Source. The studied sample was taken from the same H*P*/H*T*-synthesis as the ones used in previous experiments (Marquardt et al. 2009c; Marquardt et al. 2009d). The experiments were carried out in an externally heated diamond-anvil cell (see chapter 4.1.1) and the Brillouin scattering experiments were complemented by simultaneous measurements of x-ray diffraction from the single-crystal sample to obtain density and orientation. Figure 5.3 shows a Brillouin spectrum collected at 10 GPa and 700 K along with the x-ray diffraction spectrum, which was collected under identical conditions. The results show that increasing temperature decreases c_{11}, c_{44}, c_s, K and G, but increases c_{12} (fig. 5.4, fig. 5.5), which is in qualitative agreement with findings for MgO (Sumino et al. 1983; Isaak et al. 1989; Chen et al. 1998; Sinogeikin et al. 2000) and analogous to the effect of adding iron to MgO (Jacobsen et al. 2002; Jackson et al. 2006; Marquardt et al. 2009c; Marquardt et al. 2009d).

These first results indicate that the slowest shear wave propagating in [011], polarized along [1-10], which is determined by the shear constant c_s, is significantly lowered when temperature is increased (even if it is only increased by 400 K). The fastest shear wave propagating in [001], which is given by the constant c_{44}, is much less sensitive to temperature [as it is to pressure (Marquardt et al. 2009c; Marquardt et al. 2009d)]. This results in an increase of shear wave anisotropy of ferropericlase with increasing temperature. However, it is known that the anisotropy of ferropericlase changes sign at around 20 GPa (Karki et al. 1999; Marquardt et al. 2009d), meaning that the previously slowest shear wave propagation direction becomes the fastest. The shear anisotropy of ferropericlase in the lower mantle would than be lower along a geotherm than determined from high pressure measurements performed at ambient temperature, as it has been predicted for iron-free MgO (Karki et al. 1999). However, temperature might also affect the pressure derivative of the shear wave velocities, similar to what does the substitution of magnesium with iron (Marquardt et al. 2009d).

Bulk and shear modulus both decrease with increasing temperature and this leads to lower average velocities at high temperature (fig. 5.6) as commonly expected (e.g. Sinogeikin et al. 2004a), where the shear wave velocity is most affected by variations in temperature.

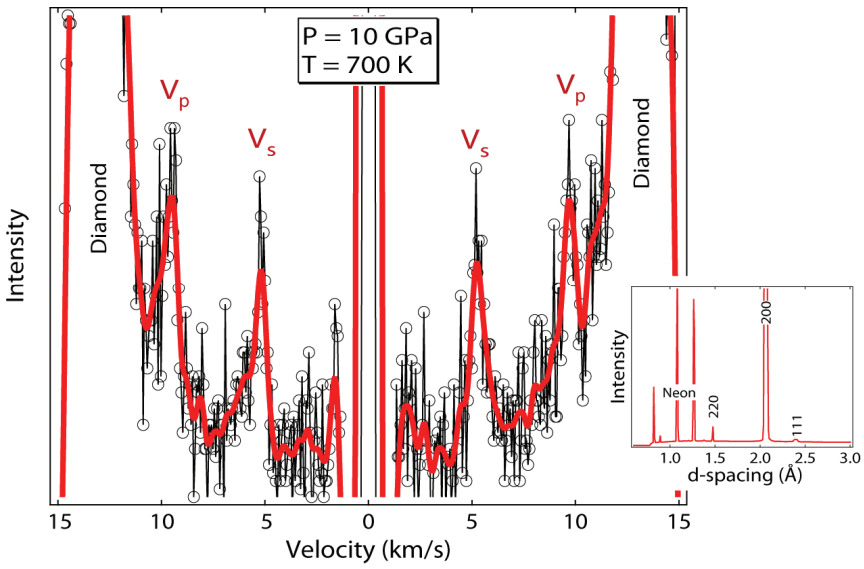

Fig. 5.3: Brillouin spectrum collected at simultaneously high-pressure and high-temperature in an externally heated diamond-anvil cell. The black circles represent the raw data and the red line (filtered) is shown for illustration. The experiment was performed at sector 13 (GSECARS) of the Advanced Photon Source. Single-crystal x-ray diffraction (inset) was collected simultaneously to determine the sample density and orientation at the same experimental conditions where Brillouin scattering was carried out.

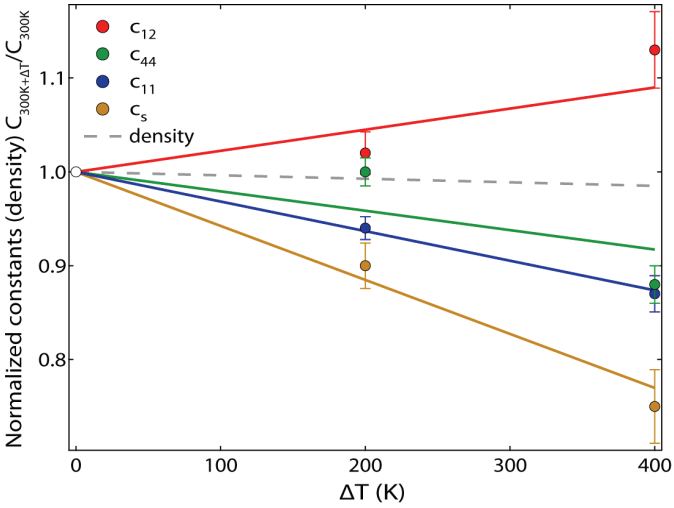

Fig. 5.4: Dependence of the elastic constants on temperature at ~10 GPa, error bars represent 1σ uncertainty. The change in normalized density is also shown. The values were determined at 500 K and 700 K and normalized to the room temperature value (at the same pressure), which was previously measured (Marquardt et al. 2009c). Except for the off-diagonal constant c_{12}, all constants decrease with increasing temperature. The different sensitivities of the shear constants c_{44} and c_s, which determine maximum and minimum shear velocity at ~10 GPa, to changes in temperature leads to stronger elastic shear anisotropy of ferropericlase at higher temperatures. Lines are weighted linear least-square fits to the experimental data.

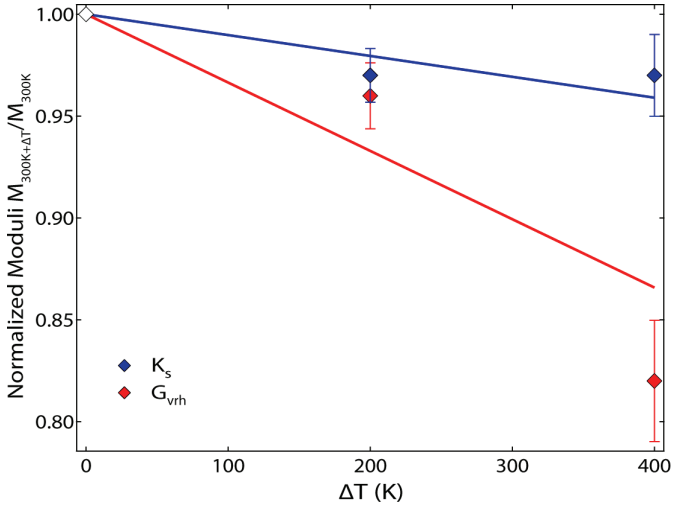

Fig. 5.5: Change of bulk and shear modulus with temperature at ~10 GPa, error bars represent 1σ uncertainty. The shear modulus is more sensitive to changes in temperature than the bulk modulus. Lines are weighted linear least-square fits to the experimental data.

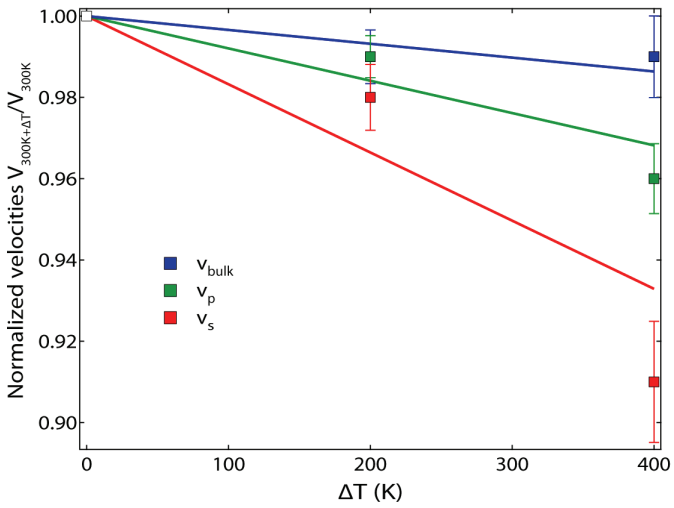

Fig. 5.6: Average velocities as a function of temperature at ~10 GPa, error bars represent 1σ uncertainty. A higher temperature leads to lower velocities and has the strongest effect on the shear velocity. Lines are weighted linear least-square fits to the experimental data.

5.4. Single-Crystal Elastic Properties of $(Y,Yb)_3Al_5O_{12}$

(This abstract is based on the following article: Marquardt, H., S. Speziale, S. Jahn, S. Ganschow and F. R. Schilling (2009). Single-Crystal Elastic Properties of $(Y,Yb)_3Al_5O_{12}$. *J. Appl. Phys.* **submitted**.)

This project aimed at a systematic understanding of the effect of chemical substitution on the elastic properties in garnet solid solution series, which are of interest for both materials science and geosciences. The studied system YAG-YbAG is of relevance for materials science, as these crystals are widely-used for solid state lasers (e.g. Patel et al., 2001; Gaumé et al., 2003), where elastic properties of the laser material are key parameters. The importance for Earth sciences arises from the fact that isostructural silicate garnets exist with varying chemical composition in the Earth's crust and mantle. Hence, a quantitative understanding of the effect of chemical variations on the physical properties, particularly elasticity, of such a closely related system can help to understand the behaviour of silicate garnets. This is needed to adequately relate geophysical observations to the properties of the constituent minerals. Garnets are ideal candidates for studying substitution-effects on elastic properties as both natural and synthetic garnets form a variety of solid solution series (see also chapter 5.1.5). In this project, the experimental Brillouin data were complemented by computations using both classical interatomic potentials and density functional theory to improve our understanding of the limitations and advantages of computational approaches for the study of single-crystal elastic properties of Earth materials.

The experimental data show that both the longitudinal and the off-diagonal constants c_{11} and c_{12} increase with increasing ytterbium content, whereas the shear constants c_{44} and $c_s = (c_{11}-c_{12})/2$ are unaffected within uncertainties (fig. 5.7). Accordingly, the bulk modulus increases with increasing ytterbium-content, but shear and Young's modulus remain constant within the experimental resolution. The observed slight increase of c_{11}, c_{12}, and K_s along the YAG-YbAG series is likely caused by the lowered oxygen-oxygen distance in YbAG compared to YAG. The substitution of the larger yttrium (ionic radius of 1.019 Å) (Shannon 1976) by the smaller ytterbium (ionic radius of 0.985 Å) (Shannon 1976) decreases the cell parameter (fig. 5.7) and the closer packing of the oxygen anions makes the material stiffer, but it does not significantly affect its shear moduli.

The experimental results indicate that changes in elastic properties along the YAG-YbAG series are of second order importance in solid sate laser design, especially in light of

the fact that other physical properties, such as thermal transport properties (Marquardt et al. 2009a) or density, change dramatically, and sometimes non-linearly (Marquardt et al. 2009a), with Y/Yb-substitution.

Interatomic potential calculations on YAG and YbAG (Schuh et al. 1991; Bush et al. 1994; Kuklja and Pandey 1999; Papagelis and Ves 2003) strongly differ from our Brillouin data. However, the more accurate and predictive DFT calculations that we performed on YAG in the present study are in good agreement with our experimental results (<10% deviation for all elastic constants, <6% deviation for aggregate elastic properties). Table 5.1 shows our experimental and computational results along with published computational data.

Table 5.1: Elastic constants c_{ij}, bulk modulus K, Young's modulus E, shear modulus G (Voigt-Reuss-Hill average) and refractive index n_{532nm} of the investigated garnets. Numbers in parenthesis indicate experimental uncertainties (1σ) in the last given digit.

Compound	c_{11} [GPa]	c_{12} [GPa]	c_{44} [GPa]	K	E	G	n_{532nm}	Method	Reference
YAG	323(3)	108(2)	115(1)	179(2)	278(3)	112(1)	1.846	Brillouin	This work
$Y_{1.83}Yb_{1.17}AG$	327(1)	109(1)	115(1)	182(1)	280(2)	113(1)	1.844	Brillouin	This work
$Y_{0.55}Yb_{2.45}AG$	328(1)	112(1)	115(1)	184(1)	280(2)	112(1)	1.859	Brillouin	This work
YbAG	332(1)	114(1)	115(1)	186(1)	282(2)	113(1)	1.858	Brillouin	This work
YAG	314	105	105	175	262	105	-	DFT (LDA)	This work
YAG	317	114	109	182	266	106	-	DFT (GGA)	This work
YbAG	312	167	102	215	235	89	-	Pair potential	This work, adopted from Bush et al. 1994
YAG	395	135	117	222	309	122	-	Pair potential	Schuh et al. 1991
YAG	330.3	164.7	131.2	220	281	109	-	Pair potential	Bush et al. 1994
YAG	340	127	112	198	278	110	-	Pair potential	Kuklja and Pandey 1999
YAG	263.3	102.4	60	156	177	67	-	Pair potential	Papagelis and Ves 2003
YbAG	263.8	98.4	63.3	154	183	70	-	Pair potential	Papagelis and Ves 2003

A better description of the elastic properties of these garnets in the framework of pair potential calculations may be obtained by using advanced interatomic potentials, as e.g. the polarizable ion model used for the simulation of melts in the Al_2O_3-Y_2O_3 system (Wilson and McMillan 2004). However, the parameters of such a model still need to be optimized, preferentially by reference to electronic structure calculations to obtain at least semi-quantitative predictions for the elastic properties, as has been shown for silicate garnets (Jahn and Madden 2007). Unfortunately, electronic structure calculations on the YbAG system are

still very challenging due to the strong electronic correlation effects arising from partially filled f-orbitals.

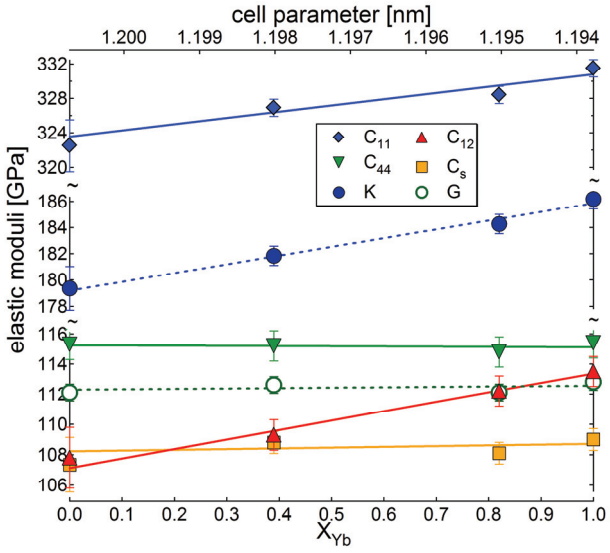

Fig. 5.7: Elastic moduli of $(Y,Yb)_3Al_5O_{12}$ as a function of ytterbium content and cell parameter. Error bars represent 1σ-uncertainty. Lines are weighted linear fits to the experimental data.

5.5. Brillouin Scattering of Natural Garnet Solid Solution Series

(article in preparation)

Minerals of the garnet group exist in a wide temperature and pressure range. This makes them one of the most abundant phases in the Earth's lower crust and upper mantle. Garnets form a variety of solid solution series and they are therefore perfect candidates to study the relation between physical properties and chemical composition (e.g. Marquardt et al. 2009a). The elastic properties of synthetic YAG-YbAG garnets are reported in Marquardt et al. 2009b. To complement the Brillouin measurements on solid solution series of synthetic garnets and to link the results to garnet systems of geophysical interest, Brillouin Scattering experiments were performed on members of the natural garnet solid solution series pyralspite (pyrope-almandine-spessartine). The chemical composition of the studied garnets as calculated from Electron Microprobe Analysis is given in table 5.2.

Table 5.2: Electron microprobe analysis of the studied natural samples reported in terms of garnet end-members (mol.%) (taken from Marquardt et al. 2009a).

Sample	Pyrope $Mg_3Al_2Si_3O_{12}$	Almandine $Fe_3Al_2Si_3O_{12}$	Spessartine $Mn_3Al_2Si_3O_{12}$	Uvarovite $Ca_3Cr_2Si_3O_{12}$	Grossular $Ca_3Al_2Si_3O_{12}$	Andradite $Ca_3Fe_2Si_3O_{12}$
AlmSpes1	0.05	45.67	53.42	0.03	0.83	0.00
GrPyrAlm1	25.66	55.99	2.91	0.04	14.18	1.23
GrAlmPyr1	50.73	37.18	1.54	0.07	10.34	0.13

Double-sided polished samples (average diameter ~1 cm, thickness ~1mm) were prepared for Brillouin scattering experiments in symmetric platelet geometry with 90° scattering angle. Velocities were collected over a 180° angular range (increments between 5° and 10°) and inverted for the three cubic elastic constants, the results are summarized in tab. 5.3.

Table 5.3: Elastic constants of three natural garnets along with adiabatic bulk modulus K_s and Voigt-Reuss-Hill averaged shear modulus G_{vrh}. The numbers in brackets represent the estimated uncertainty in the last reported digit. The density is taken from Marquardt et al. 2009a.

Sample	ρ (g/cm³)	c_{11} (GPa)	c_{12} (GPa)	c_{44} (GPa)	K_s (GPa)	G_{vrh} (GPa)
AlmSpes1	4.25	306(2)	112(2)	94(2)	177(2)	95(2)
GrPyrAlm1	3.84	300(2)	107(2)	94(2)	171(2)	95(2)
GrAlmPyr1	4.00	304(2)	109(2)	95(2)	174(2)	96(2)

In order to simplify this natural system and make it comparable to the binary solid solution series of the synthetic garnets, a fictive solid solution series between pyrope and almandine + spessartine is introduced (Marquardt et al. 2009a). This assumption is based on the similar atomic masses of Mn and Fe. Figure 5.8 shows the dependence of elastic constants on the chemical composition, which is represented as pyrope-content. The shear constants c_{44}, c_s and G_{vrh} are independent of composition within uncertainties, whereas the constants c_{11}, c_{12}, and K_s slightly change with Fe(Mn)/Mg-substitution; this is comparable to the observations for synthetic garnets. This behaviour is likely caused by either the mass-difference or the size difference of the exchanging ions (see also Marquardt et al. 2009b). Comparison of the results on pyralspite garnets with the data collected on the YAG-YbAG series can help to understand the dominating cause for the change of elastic constants. In the case of Fe(Mn)-Mg-exchange, both atomic mass and ionic radius increase (Fe and Mn are larger and heavier than Mg), whereas for Y/Yb-substitution size and mass are inversely correlated, i.e. Yb is smaller and heavier than Y. The bulk modulus decreases when Fe (or Mn) and Yb are substituted by Mg

and Y, respectively (the lighter atoms) (fig. 5.9). Based on figure 5.9, one may conclude that the primary cause for changes in elastic properties along the studied garnet solid series is most likely the difference of atomic mass and the ionic radius is only a second order effect. This is contrary to the interpretation in Marquardt et al. 2009b, which was based on the results of the synthetic garnets only. However, in both systems the relative mass difference between the exchanged ions is much larger than the difference in ionic radius – this could also explain the apparent dominance of mass over size. The results emphasize the potential of combining data sets on different chemical systems within the same structural mineral group, but also indicate the need for additional systematic data sets, particularly on high-quality synthetic solution series. It could, for instance, be of interest to substitute ytterbium with different lanthanoids, where the associated relative changes in atomic mass and ionic radius are comparable in magnitude.

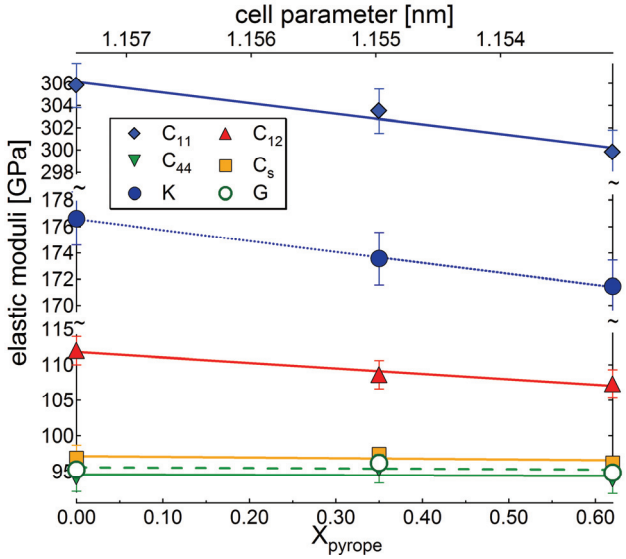

Fig. 5.8: Dependence of the elastic properties on pyrope (i.e. Mg) content and cell parameter (from Marquardt et al. 2009a). The constants c_{11}, c_{12} (and K_s) decrease with increasing pyrope content. The shear constants c_{44}, c_s (and G_{vrh}) are unaffected. Error bars represent 1σ uncertainty. Lines are weighted linear least-square fits to the experimental data.

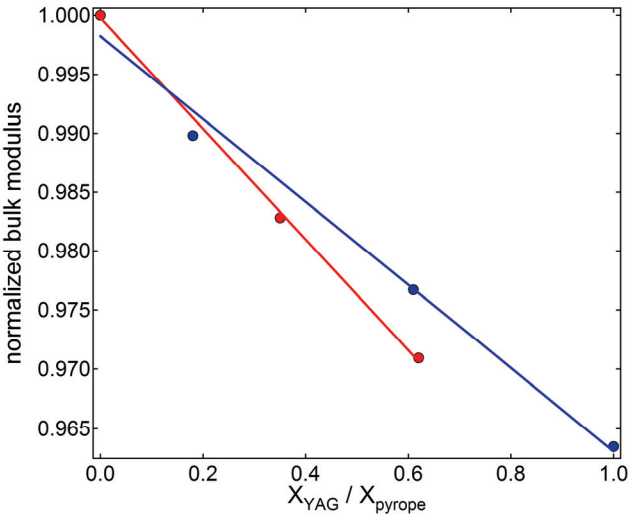

Fig. 5.9: Normalized bulk modulus of garnets as a function of pyrope (i.e. Mg) content (red) or YAG content (blue). The bulk modulus decreases when Fe and Yb are substituted by Mg and Y, respectively. Lines are linear least-square fits to the experimental data.

According to earlier studies (Bass 1986; Duffy and Anderson 1989; Wang and Ji 2001), the bulk sound velocity $V_\Phi = (K/\rho)^{0.5}$ is in a simple way related to the mean atomic weight of garnets M and can be described by $V_\Phi M^n = k$ where n and k are constants. Fitting the data of the natural pyralspite garnets to the above equation yields k = 18.7(±3.5) km $g^{0.33}$/s, n = 0.33(±0.06) (fig. 5.10), in agreement with the fit parameters k = 20.26 km $g^{0.36}$/s and n = 0.36 reported previously (Wang and Ji 2001). For the YAG-YbAG system, k = 31.6(±2) km $g^{0.48}$/s and n = 0.48(±0.02) are derived, which is in between the values that were reported for pyralspite and ugrandite (uvarovite-grossulare-andradite) silicate garnets (Wang and Ji 2001).

These findings suggest that elasticity systematics of garnets are, at least to some extent, transferable between different chemical systems. Future studies on other garnet solution series, both synthetic and natural, at high-pressures and high-temperatures can reveal more details about elasticity systematics and sound wave velocity relations in isostructural compounds at conditions relevant to the Earth's deep interior.

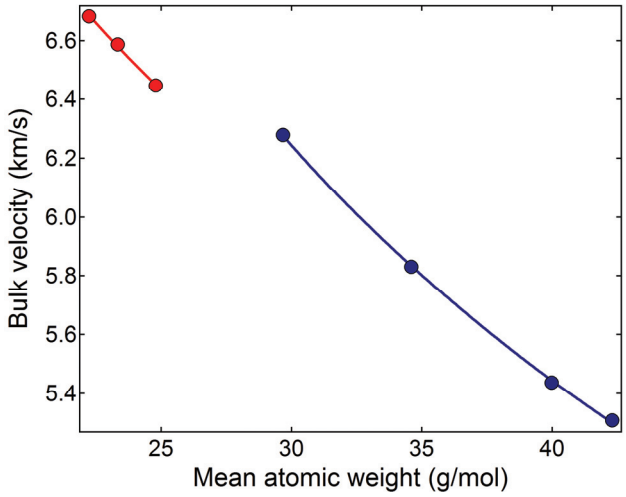

Fig 5.10: bulk sound velocity as a function of mean atomic weight. The slope in the diagram is different for aluminium garnets (blue circles) and silicate (red circles) garnets. Curves are least-square fits to the empirical equation $V_\Phi M^n = k$ (Bass 1986; Duffy and Anderson 1989; Wang and Ji 2001).

References

Abramson, E. H., J. M. Brown and L. J. Slutsky (1999). Applications of impulsive stimulated scattering in the earth and planetary sciences. *Annu. Rev. Phys. Chem.* **50**: 279-313.

Anderson, D. L. (1989). *Theory of the Earth*, Blackwell Science Ltd.

Anderson, O. L. and D. G. Isaak (1995). Elastic constants of mantle minerals at high temperature. *Mineral physics and crystallography; a handbook of physical constants*. Washington, DC, United States, American Geophysical Union**:** 64-97.

Angel, R. J., M. Bujak, J. Zhao, G. D. Gatta and S. D. Jacobsen (2007). Effective hydrostatic limits of pressure media for high-pressure crystallographic studies. *J. Appl. Crystallogr.* **40**: 26-32.

Angel, R. J., J. M. Jackson, H. J. Reichmann and S. Speziale (2009). Elasticity measurements on minerals: A review. *Eur. J. Mineral.*: DOI: 10.1127/0935-1221/2009/0021-1925.

Antonangeli, D., M. Krisch, G. Fiquet, D. L. Farber, C. M. Aracne, J. Badro, F. Occelli and H. Requardt (2004a). Elasticity of Cobalt at High Pressure Studied by Inelastic X-Ray Scattering. *Phys. Rev. Lett.* **93**: 215505.

Antonangeli, D., F. Occelli, H. Requardt, J. Badro, G. Fiquet and M. Krisch (2004b). Elastic anisotropy in textured hcp-iron to 112 GPa from sound wave propagation measurements. *Earth Planet. Sci. Lett.* **225**: 243-251.

Askarpour, V., M. H. Manghnani, S. Fassbender and A. Yoneda (1993). Elasticity of single-crystal $MgAlO_4$ spinel up to 1273 K by Brillouin spectroscopy. *Phys. Chem. Miner.* **19**: 511-519.

Badro, J., G. Fiquet, F. Guyot, J.-P. Rueff, V. V. Struzhkin, G. Vanko and G. Monaco (2003). Iron partitioning in Earth's mantle: toward a deep lower mantle discontinuity. *Science* **300**: 789-791.

Badro, J., J.-P. Rueff, G. Vanko, G. Monaco, G. Fiquet and F. Guyot (2004). Electronic Transitions in Perovskite: Possible Nonconvecting Layers in the Lower Mantle. *Science* **305**: 383-386.

Bass, J. D. (1986). Elasticity of uvarovite and andradite garnets. *J. Geophys. Res. B* **91**: 7505-7516.

Bass, J. D. (1989). Elasticity of grossular and spessartite garnets by Brillouin spectroscopy. *J. Geophys. Res. B* **94**: 7621-7628.

Bass, J. D. (2007). Techniques for measuring High *P*/*T* Elasticity. *Treatise on Geophysics - Mineral Physics*. G. D. Price. Amsterdam, Elsevier.

Bina, C. R., D. H. Heinrich and K. T. Karl (2003). Seismological Constraints upon Mantle Composition. *Treatise on Geochemistry*. Oxford, Pergamon**:** 39-59.

Birch, F. (1938). The Effect of Pressure Upon the Elastic Parameters of Isotropic Solids, According to Murnaghan's Theory of Finite Strain. *J. Appl. Phys.* **9**: 279-288.

Boehler, R. (1992). Melting of the Fe-FeO and Fe-FeS systems at high pressure; constraints on core temperatures. *Earth Planet. Sci. Lett.* **111**: 217-227.

Boehler, R. (2000). Laser heating in the diamond cell: techniques and applications. *Hyperfine Interact.* **128**: 307-321.

Brillouin, L. (1922). *Annalen der Physik (Paris)* **88**: 17.

Brown, J. M. and R. G. McQueen (1986). Phase Transitions, Grüneisen Parameter, and Elasticity for Shocked Iron Between 77 GPa and 400 GPa. *J. Geophys. Res.* **91**: 7485–7494.

Brown, J. M. and T. J. Shankland (1981). Thermodynamic parameters in the Earth as determined from seismic profiles. *Geophys. J. Roy. Astr. S.* **66**: 579-596.

Bullen, K. E. (1947). *An Introduction to the Theory of Seismology*, Cambridge University Press.

Bullen, K. E. (1949). Compressibility-Pressure Hypothesis and the Earth's Interior. *Geophys. J. Int.* **5**: 335-368.

Burkel, E. (2000). Phonon spectroscopy by inelastic x-ray scattering. *Rep. Prog. Phys*: 171.

Burkel, E. (2001). Determination of phonon dispersion curves by means of inelastic x-ray scattering. *J. Phys. Condens. Matter* **13**: 7627.

Bush, T. S., J. D. Gale, C. R. A. Catlow and P. D. Battle (1994). Self-consistent interatomic potentials for the simulation of binary and ternary oxides. *J. Mater. Chem.* **4**: 831-837.

Cammarano, F., S. Goes, A. Deuss and D. Giardini (2005). Is a pyrolitic adiabatic mantle compatible with seismic data? *Earth Planet. Sci. Lett.* **232**: 227-243.

Chen, G., R. C. Liebermann and D. J. Weidner (1998). Elasticity of Single-Crystal MgO to 8 Gigapascals and 1600 Kelvin. *Science* **280**: 1913-1916.

Crowhurst, J. C., J. M. Brown, A. F. Goncharov and S. D. Jacobsen (2008). Elasticity of (Mg,Fe)O through the spin transition of iron in the lower mantle. *Science* **319**: 451-453.

Crowhurst, J. C., A. F. Goncharov, J. M. Zaug, C. Jiuhua, W. Yanbin, S. D. Thomas, S. Guoyin and F. D. Larissa (2005). Direct measurements of the elastic properties of iron and cobalt to 120 GPa--implications for the composition of earth's core. *Advances in High-Pressure Techniques for Geophysical Applications*. Amsterdam, Elsevier**:** 3-23.

Crowhurst, J. C., G. R. Hearne, J. D. Comins, A. G. Every and P. R. Stoddart (1999). Surface Brillouin scattering at high pressure: Application to a thin supported gold film. *Phys. Rev. B* **60**: R14990.

Crowhurst, J. C. and J. M. Zaug (2004). Surface acoustic waves in germanium single crystals. *Phys. Rev. B* **69**: 052301.

Crowhurst, J. C., J. M. Zaug, E. H. Abramson, J. M. Brown and D. W. Ahre (2003). Impulsive Stimulated Light Scattering at High Pressure - Precise Determination of Elastic Constants of Opaque Materials. *High Press. Res.* **23**: 373-377.

Cummins, H. Z. and P. E. Schoen (1972). Linear scattering from thermal fluctuations. *Laser handbook*. F. T. Arecchi and E. O. Schultz-DuBois. Amsterdam, North Holland Publishing Co.

Da Silva, C. R. S., R. M. Wentzcovitch, Z. Wu and J. Justo (2008). Potential effects of the spin crossover transition in ferropericlase on mantle velocities. *Eos Trans. AGU* **89**: Fall Meet. Suppl., Abstract MR23A-10.

Davies, G. F. (1974). Effective elastic moduli under hydrostatic stress - I. quasi-harmonic theory. *J. Phys. Chem. Solids* **35**: 1513-1520.

Dorogokupets, P. I. and A. R. Oganov (2007). Ruby, metals, and MgO as alternative pressure scales: A semiempirical description of shock-wave, ultrasonic, x-ray, and thermochemical data at high temperatures and pressures. *Phys. Rev. B* **75**: 024115-024116.

Dubrovinsky, L., N. Dubrovinskaia, O. Narygina, I. Kantor, A. Kuznetzov, V. B. Prakapenka, L. Vitos, B. Johansson, A. S. Mikhaylushkin, S. I. Simak and I. A. Abrikosov (2007). Body-Centered Cubic Iron-Nickel Alloy in Earth's Core. *Science* **316**: 1880-1883.

Dubrovinsky, L. S., N. A. Dubrovinskaia, S. K. Saxena, H. Annersten, E. Halenius, H. Harryson, F. Tutti, S. Rekhi and T. L. Bihan (2000). Stability of Ferropericlase in the Lower Mantle. *Science* **289**: 430-432.

Duffy, T. S. and T. J. Ahrens (1995). Compressional sound velocity, equation of state, and constitutive response of shock-compressed magnesium oxide. *J. Geophys. Res.* **100**: 529-542.

Duffy, T. S. and D. L. Anderson (1989). Seismic velocities in mantle minerals and the mineralogy of the upper mantle. *J. Geophys. Res. B* **94**: 1895-1912.

Duffy, T. S., R. J. Hemley and H.-k. Mao (1995a). Equation of State and Shear Strength at Multimegabar Pressures: Magnesium Oxide to 227 GPa. *Phys. Rev. Lett.* **74**: 1371.

Duffy, T. S., C.-s. Zha, R. T. Downs, H.-k. Mao and R. J. Hemley (1995b). Elasticity of forsterite to 16 GPa and the composition of the upper mantle. *Nature* **378**: 170-173.

Dziewonski, A. M. and D. L. Anderson (1981). Preliminary reference Earth model. *Phys. Earth Planet. Inter.* **25**: 297-356.

Every, A. G. (1980). General closed-form expressions for acoustic waves in elastically anisotropic solids. *Phys. Rev. B* **22**: 1746.

Fei, Y., A. Ricolleau, M. Frank, K. Mibe, G. Shen and V. Prakapenka (2007a). High-Pressure Geoscience Special Feature: Toward an internally consistent pressure scale. *Proc. Natl. Acad. Sci.* **104**: 9182-9186.

Fei, Y., L. Zhang, A. Corgne, H. Watson, A. Ricolleau, Y. Meng and V. Prakapenka (2007b). Spin transition and equations of state of (Mg,Fe)O solid solutions. *Geophys. Res. Lett.* **34**: L17307.

Fiquet, G., J. Badro, F. Guyot, C. Bellin, M. Krisch, D. Antonangeli, H. Requardt, A. Mermet, D. Farber, C. Aracne-Ruddle and J. Zhang (2004). Application of inelastic X-ray scattering to the measurements of acoustic wave velocities in geophysical materials at very high pressure. *Phys. Earth Planet. Inter.* **143-144**: 5-18.

Fiquet, G., J. Badro, F. Guyot, H. Requardt and M. Krisch (2001). Sound Velocities in Iron to 110 Gigapascals. *Science* **291**: 468-471.

Fischer, K. M. (2002). Earth science: Flow and fabric deep down. *Nature* **415**: 745-748.

Frost, D. J. (2008). The upper mantle and transition zone. *Elements* **4**: 171-176.

Frost, D. J., B. T. Poe, R. G. Trønnes, C. Liebske, A. Duba and D. C. Rubie (2004). A new large-volume multianvil system. *Phys. Earth Planet. Inter.* **143-144**: 507-514.

Fyfe, W. S. (1960). The possibility of d-electron coupling in olivine at high pressures. *Geochim. Cosmochim. Acta* **19**: 141-143.

Garnero, E. J., V. Maupin, T. Lay and M. J. Fouch (2004). Variable azimuthal anisotropy in Earth's lowermost mantle. *Science* **306**: 259-261.

Garnero, E. J. and A. K. McNamara (2008). Structure and dynamics of Earth's lower mantle. *Science* **320**: 626-628.

Goncharov, A. F., J. Crowhurst and J. M. Zaug (2004). Elastic and Vibrational Properties of Cobalt to 120 GPa. *Phys. Rev. Lett.* **92**: 115502.

Grimsditch, M. (2001). Brillouin Scattering. *Handbook of Elastic Properties of Solids, Liquids, and Gases. Volume I: Dynamic Methods for Measuring the Elastic Properties of Solids*. Levy, Bass and Stern, Academic Press.

Gross, E. (1930). Change of Wave-length of light due to elastic heat waves at scattering of liquids. *Nature* **126**: 201.

Gwanmesia, G. D., L. Wang, R. Triplett and R. C. Liebermann (2008). Pressure and temperature dependence of the elasticity of pyrope-majorite ($Py_{60}Mj_{40}$ and $Py_{50}Mj_{50}$) garnets solid solution measured by ultrasonic interferometry technique. *Phys. Earth Planet. Inter.* **In Press, Corrected Proof**.

Gwanmesia, G. D., J. Zhang, K. Darling, J. Kung, B. Li, L. Wang, D. Neuville and R. C. Liebermann (2006). Elasticity of polycrystalline pyrope ($Mg_3Al_2Si_3O_{12}$) to 9 GPa and 1000 °C. *Phys. Earth Planet. Inter.* **155**: 179-190.

Hashin, Z. and S. Shtrikman (1962). A variational approach to the theory of the elastic behaviour of polycrystals. *J. Mech. Phys. Solids* **10**: 343-352.

Hess, H. H. (1964). Seismic Anisotropy of the Uppermost Mantle under Oceans. *Nature* **203**: 629-631.

Higo, Y., T. Inoue, T. Irifune, K.-i. Funakoshi and B. Li (2008). Elastic wave velocities of $(Mg_{0.91}Fe_{0.09})_2SiO_4$ ringwoodite under P-T conditions of the mantle transition region. *Phys. Earth Planet. Inter.* **166**: 167-174.

Hill, R. (1952). The elastic behaviour of a crystalline aggregate. *Proc Phys Soc Lond A* **65**: 349-354.

Holzapfel, W. B. (2003). Refinement of the ruby luminescence pressure scale. *J. Appl. Phys.* **93**: 1813-1818.

Hu, M. Y., W. Sturhahn, T. S. Toellner, P. D. Mannheim, D. E. Brown, J. Zhao and E. E. Alp (2003). Measuring velocity of sound with nuclear resonant inelastic x-ray scattering. *Phys. Rev. B* **67**: 094304.

Hutko, A. R., T. Lay, J. Revenaugh and E. J. Garnero (2008). Anticorrelated Seismic Velocity Anomalies from Post-Perovskite in the Lowermost Mantle. *Science* **320**: 1070-1074.

Irifune, T., M. Isshiki and S. Sakamoto (2005). Transmission electron microscope observation of the high-pressure form of magnesite retrieved from laser heated diamond anvil cell. *Earth Planet. Sci. Lett.* **239**: 98-105.

Isaak, D. G., O. L. Anderson and T. Goto (1989). Measured elastic moduli of single-crystal MgO up to 1800 K. *Phys. Chem. Miner.* **16**: 704-713.

Ito, E. (2006). Sintered diamond multi anvil apparatus and its application to mineral physics. *J. Miner. Petrol. Sci.* **101**: 118-121.

Ito, E. (2007). Multianvil Cells and High-Pressure Experimental Methods. *Treatise on Geophysics - Mineral Physics*. G. D. Price. Amsterdam, Elsevier.

Ito, E., T. Katsura, D. Yamazaki, A. Yoneda, M. Tado, T. Ochi, E. Nishibara and A. Nakamura (2008). A new 6-axis apparatus to squeeze the Kawai-cell of sintered diamond cubes. *Phys. Earth Planet. Inter.* **In Press, Corrected Proof**.

Jackson, I., S. K. Khanna, A. Revcolevschi and J. Berthon (1990). Elasticity, shear-mode softening and high-pressure polymorphism of wuestite ($Fe_{1-x}O$). *J. Geophys. Res.* **95**: 21,671-621,685.

Jackson, I., H. Niesler and D. J. Weidner (1981). Explicit Correction of Ultrasonically Determined Elastic Wave Velocities for Transducer-bond Phase Shifts. *J. Geophys. Res.* **86**: 3736–3748.

Jackson, J. M., S. V. Sinogeikin and J. D. Bass (2000). Sound velocities and elastic properties of gamma-Mg_2SiO_4 to 873 K by Brillouin spectroscopy. *Am. Mineral.* **85**: 296-303.

Jackson, J. M., S. V. Sinogeikin and J. D. Bass (2007). Sound velocities and single-crystal elasticity of orthoenstatite to 1073 K at ambient pressure. *Phys. Earth Planet. Inter.* **161**: 1-12.

Jackson, J. M., S. V. Sinogeikin, S. D. Jacobsen, H. J. Reichmann, S. J. Mackwell and J. D. Bass (2006). Single-crystal elasticity and sound velocities of $(Mg_{0.94}Fe_{0.06})O$ ferropericlase to 20 GPa. *J. Geophys. Res.* **111**: B09203.

Jackson, J. M., J. Zhang and J. D. Bass (2004). Sound velocities and elasticity of aluminous $MgSiO_3$ perovskite; implications for aluminum heterogeneity in Earth's lower mantle. *Geophys. Res. Lett.* **31**: L10614.

Jacobsen, S. D., H. J. Reichmann, H. Spetzler, S. J. Mackwell, J. R. Smyth, R. J. Angel and C. A. McCammon (2002). Structure and elasticity of single-crystal (Mg,Fe)O and a new method of generating shear waves for gigahertz ultrasonic interferometry. *J. Geophys. Res.* **107**: 2037.

Jacobsen, S. D., H. Spetzler, H. J. Reichmann and J. R. Smyth (2004). Shear waves in the diamond-anvil cell reveal pressure-induced instability in (Mg,Fe)O. *Proc. Natl. Acad. Sci.* **101**: 5867-5871.

Jahn, S. and P. A. Madden (2007). Modeling Earth materials from crustal to lower mantle conditions; a transferable set of interaction potentials for the CMAS system. *Phys. Earth Planet. Inter.* **162**: 129-139.

Jayaraman, A. (1983). Diamond anvil cell and high-pressure physical investigations. *Rev. Mod. Phys.* **55**: 65.

Kantor, A. P., I. Y. Kantor, A. V. Kurnosov, A. Y. Kuznetsov, N. A. Dubrovinskaia, M. Krisch, A. A. Bossak, V. P. Dmitriev, V. S. Urusov and L. S. Dubrovinsky (2007). Sound wave velocities of fcc Fe-Ni alloy at high pressure and temperature by mean of inelastic X-ray scattering. *Phys. Earth Planet. Inter.* **164**: 83-89.

Karato, S.-i. (1989). Plasticity-crystal structure systematics in dense oxides and its implications for the creep strength of the Earth's deep interior: a preliminary result. *Phys. Earth Planet. Inter.* **55**: 234-240.

Karato, S.-i., S. Zhang and H.-R. Wenk (1995). Superplasticity in Earth's Lower Mantle: Evidence from Seismic Anisotropy and Rock Physics. *Science* **270**: 458-461.

Karato, S. i. and B. B. Karki (2001). Origin of lateral variation of seismic wave velocities and density in the deep mantle. *J. Geophys. Res. B* **106**: 21,771-721,783.

Karki, B. B., L. Stixrude, S. J. Clark, M. C. Warren, G. J. Ackland and J. Crain (1997). Elastic properties of orthorhombic $MgSiO_3$ perovskite at lower mantle pressures. *Am. Mineral.* **82**: 635-638.

Karki, B. B., L. Stixrude and R. M. Wentzcovitch (2001). High-pressure elastic properties of major materials of Earth's mantle from first principles. *Rev. Geophys.* **39**: 507-534.

Karki, B. B., R. M. Wentzcovitch, S. de Gironcoli and S. Baroni (1999). First-principles determination of elastic anisotropy and wave velocities of MgO at lower mantle conditions. *Science* **286**: 1705-1707.

Katsura, T., K.-i. Funakoshi, A. Kubo, N. Nishiyama, Y. Tange, Y.-i. Sueda, T. Kubo and W. Utsumi (2004). A large-volume high-pressure and high-temperature apparatus for in situ X-ray observation, `SPEED-Mk.II'. *Phys. Earth Planet. Inter.* **143-144**: 497-506.

Katsura, T. and E. Ito (1989). The System Mg_2SiO_4-Fe_2SiO_4 at High Pressures and Temperatures: Precise Determination of Stabilities of Olivine, Modified Spinel, and Spinel. *J. Geophys. Res.* **94**: 15,663–615,670.

Katsura, T., K. Sato and E. Ito (1998). Electrical conductivity of silicate perovskite at lower-mantle conditions. *Nature* **395**: 493-495.

Kendall, J. M. and P. G. Silver (1996). Constraints from seismic anisotropy on the nature of the lowermost mantle. *Nature* **381**: 409-412.

Kenichi, T. (2001). Evaluation of the hydrostaticity of a helium-pressure medium with powder x-ray diffraction techniques. *J. Appl. Phys.* **89**: 662-668.

Kennett, B. L. N., E. R. Engdahl and R. Buland (1995). Constraints on seismic velocities in the Earth from traveltimes. *Geophys. J. Int.* **122**: 108-124.

Keppler, H., L. S. Dubrovinsky, O. Narygina and I. Kantor (2008). Optical Absorption and Radiative Thermal Conductivity of Silicate Perovskite to 125 Gigapascals. *Science* **322**: 1529-1532.

Keppler, H., I. Kantor and L. Dubrovinsky (2007). Optical absorption of ferropericlase to 84 GPa. *Am. Mineral.* **92**: 433-436.

Keppler, H. and J. R. Smyth (2005). Optical and near infrared spectra of ringwoodite to 21.5 GPa: Implications for radiative heat transport in the mantle. *Am. Mineral.* **90**: 1209-1212.

Koci, L., L. Vitos and R. Ahuja (2007). Ab initio calculations of the elastic properties of ferropericlase $Mg_{1-x}Fe_xO$ (x<=0.25). *Phys. Earth Planet. Inter.* **164**: 177-185.

Kuklja, M. M. and R. Pandey (1999). Atomistic Modeling of Native Point Defects in Yttrium Aluminium Garnet Crystals. *J. Am. Ceram. Soc.* **82**: 2881-2886.

Kurnosov, A., I. Kantor, T. Boffa-Ballaran, S. Lindhardt, L. Dubrovinsky, A. Kuznetsov and B. H. Zehnder (2008). A novel gas-loading system for mechanically closing of various types of diamond anvil cells. *Rev. Sci. Instrum.* **79**: 045110-045115.

Lay, T., Q. Williams and E. J. Garnero (1998). The core-mantle boundary layer and deep Earth dynamics. *Nature* **392**: 461-468.

Lee, K. K. M., B. O'Neill, W. R. Panero, S.-H. Shim, L. R. Benedetti and R. Jeanloz (2004). Equations of state of the high-pressure phases of a natural peridotite and implications for the Earth's lower mantle. *Earth Planet. Sci. Lett.* **223**: 381-393.

Li, B., R. C. Liebermann and D. J. Weidner (1998). Elastic Moduli of Wadsleyite (beta-Mg_2SiO_4) to 7 Gigapascals and 873 Kelvin. *Science* **281**: 675-677.

Lin, J.-F., S. D. Jacobsen, W. Sturhahn, J. M. Jackson, J. Zhao and C.-S. Yoo (2006). Sound velocities of ferropericlase in the Earth`s lower mantle. *Geophys. Res. Lett.* **33**: L22304.

Lin, J.-F., V. V. Struzhkin, S. D. Jacobsen, M. Y. Hu, P. Chow, J. Kung, H. Liu, H.-k. Mao and R. J. Hemley (2005a). Spin transition of iron in magnesiowüstite in the Earth's lower mantle. *Nature* **436**: 377-380.

Lin, J.-F. and T. Tsuchiya (2008). Spin transition of iron in the Earth's lower mantle. *Phys. Earth Planet. Inter.* **170**: 248-259.

Lin, J.-F., G. Vanko, S. D. Jacobsen, V. Iota, V. V. Struzhkin, V. B. Prakapenka, A. Kuznetsov and C.-S. Yoo (2007). Spin Transition Zone in Earth's Lower Mantle. *Science* **317**: 1740-1743.

Lin, J.-F., H. Watson, G. Vanko, E. E. Alp, V. B. Prakapenka, P. Dera, V. V. Struzhkin, A. Kubo, J. Zhao, C. McCammon and W. J. Evans (2008). Intermediate-spin ferrous iron in lowermost mantle post-perovskite and perovskite. *Nature Geoscience* **1**: 688-691.

Lin, J. F., W. Sturhahn, J. Zhao, G. Shen, H. k. Mao and R. J. Hemley (2005b). Sound velocities of hot dense iron; Birch's law revisited. *Science* **308**: 1892-1894.

Liu, W., J. Kung and B. Li (2005). Elasticity of San Carlos olivine to 8 GPa and 1073 K. *Geophys. Res. Lett.* **32**: L16301.

Long, M. D., X. Xiao, Z. Jiang, B. Evans and S.-i. Karato (2006). Lattice preferred orientation in deformed polycrystalline (Mg,Fe)O and implications for seismic anisotropy in D". *Phys. Earth Planet. Inter.* **156**: 75-88.

Madi, K., S. Forest, P. Cordier and M. Boussuge (2005). Numerical study of creep in two-phase aggregates with a large rheology contrast: implications for the lower mantle. *Earth Planet. Sci. Lett.* **237**: 223-238.

Mainprice, D. and M. Humbert (1994). Methods of calculating petrophysical properties from lattice preferred orientation data. *Seismic properties of crustal and mantle rocks; laboratory measurements and theoretical calculations*. Dordrecht-Boston, International, D Reidel Publishing Company. **15; 5:** 575-592.

Mandelstam, L. I. (1926). *Jour Russ Phys-Chem Soc* **58**: 831.

Mao, H.-k. and P. M. Bell (1972). Electrical Conductivity and the Red Shift of Absorption in Olivine and Spinel at High Pressure. *Science* **176**: 403-406.

Mao, H.-k., P. M. Bell, J. W. Shaner and D. J. Steinberg (1978). Specific volume measurements of Cu, Mo, Pd, and Ag and calibration of the ruby R_1 fluorescence pressure gauge from 0.06 to 1 Mbar. *J. Appl. Phys.* **49**: 3276-3283.

Mao, H.-k., R. J. Hemley, L. C. Chen, J. F. Shu, L. W. Finger and Y. Wu (1989). X-ray Diffraction to 302 Gigapascals: High-Pressure Crystal Structure of Cesium Iodide. *Science* **246**: 649-651.

Mao, H.-k., Y. Wu, L. C. Chen, J. F. Shu and A. P. Jephcoat (1990). Static compression of iron to 300 GPa and $Fe_{0.8}Ni_{0.2}$ alloy to 260 GPa; implications for composition of the core. *J. Geophys. Res.* **95**: 21,737-721,742.

Mao, H.-k., J. Xu and P. M. Bell (1986). Calibration of the ruby pressure gauge to 800 kbar under quasi-hydrostatic conditions. *J. Geophys. Res.* **91**: 4673-4676.

Mao, H.-k., J. Xu, V. V. Struzhkin, J. Shu, R. J. Hemley, W. Sturhahn, M. Y. Hu, E. E. Alp, L. Vocadlo, D. Alfe, G. D. Price, M. J. Gillan, M. Schwoerer-Bohning, D. Hausermann, P. Eng, G. Shen, H. Giefers, R. Lubbers and G. Wortmann (2001). Phonon Density of States of Iron up to 153 Gigapascals. *Science* **292**: 914-916.

Mao, H. k. and W. L. Mao (2007). Diamond-Anvil Cells and Probes for High *P-T* Mineral Physics Studies. *Treatise on Geophysics - Mineral Physics*. G. D. Price. Amsterdam, Elsevier.

Marquardt, H., S. Ganschow and F. Schilling (2009a). Thermal diffusivity of natural and synthetic garnet solid solution series. *Phys. Chem. Miner.* **36**: 107-118.

Marquardt, H., S. Speziale, S. Jahn, S. Ganschow and F. R. Schilling (2009b). Single-Crystal Elastic Properties of $(Y,Yb)_3Al_5O_{12}$. *J. Appl. Phys.* **submitted**.

Marquardt, H., S. Speziale, H. J. Reichmann, D. J. Frost and F. R. Schilling (2009c). Single-Crystal Elastic Properties of $(Mg_{0.9}Fe_{0.1})O$ to 81 GPa. *Earth Planet. Sci. Lett.* **submitted**.

Marquardt, H., S. Speziale, H. J. Reichmann, D. J. Frost, F. R. Schilling and E. J. Garnero (2009d). Elastic Shear Anisotropy of Ferropericlase in Earth's Lower Mantle. *Science* **324**: 224-226.

Marquardt, H., S. Speziale, H. J. Reichmann and F. R. Schilling (2007). Brillouin Spectroscopy at GeoForschungsZentrum Potsdam: Applications in Geoscience and Materials Science. *Eos Trans. AGU* **88**: Fall Meet. Suppl., Abstract MR43C-1521.

Masters, G., G. Laske, H. Bolton and A. Dziewonski (2000). The Relative Behavior of Shear Velocity, Bulk Sound Speed, and Compressional Velocity in the Mantle: Implications for Chemical and Thermal Structure. *Geophysical Monograph 117: Earth's Deep Interior: Mineral Physics and Tomography, From Atomic to Global Scale*. S.-i. Karato, A. Forte, R. C. Liebermann, G. Masters and L. Stixrude. Washington, DC, American Geophysical Union.

McCammon, C., I. Kantor, O. Narygina, J. Rouquette, U. Ponkratz, I. Sergueev, M. Mezouar, V. Prakapenka and L. Dubrovinsky (2008a). Stable intermediate-spin ferrous iron in lower-mantle perovskite. *Nature Geoscience* **1**: 684-687.

McCammon, C. A., L. Dubrovinsky, I. Kantor, O. Narygina, X. Wu, A. Chumakov and I. Sergeev (2008b). Elastic Wave Velocities of Lower Mantle Perovskite With Intermediate-spin Iron and Consequences for Mantle Properties and Dynamics. *Eos Trans. AGU* **89**: Fall Meet. Suppl., Abstract MR23A-07.

McNamara, A. K., P. E. van Keken and S.-I. Karato (2002). Development of anisotropic structure in the Earth's lower mantle by solid-state convection. *Nature* **416**: 310-314.

Mizukami, T., S. R. Wallis and J. Yamamoto (2004). Natural examples of olivine lattice preferred orientation patterns with a flow-normal a-axis maximum. *Nature* **427**: 432-436.

Mueller, H. J., C. Lathe and F. R. Schilling (2005). Simultaneous determination of elastic and structural properties under simulated mantle conditions using multi-anvil device MAX80. *Advances in High-Pressure Techniques for Geophysical Applications*. J. Chen, Y. Wang, T. S. Duffy, G. Shen and L. P. Dobrzhinetskaya. Amsterdam, Elsevier.

Mueller, H. J., J. Lauterjung, F. R. Schilling, C. Lathe and G. Nover (2002). Symmetric and asymmetric interferometric method for ultrasonic compressional and shear wave velocity measurements in piston-cylinder and multi-anvil high-pressure apparatus. *Eur. J. Mineral.* **14**: 581-589.

Mueller, H. J., F. R. Schilling, J. Lauterjung and C. Lathe (2003). A standard-free pressure calibration using simultaneous XRD and elastic property measurements in a multi-anvil device. *Eur. J. Mineral.* **15**: 865-873.

Murakami, M., Y. Asahara, Y. Ohishi, N. Hirao and K. Hirose (2008). Development of in situ Brillouin spectroscopy at high pressure and high temperature with synchrotron radiation and infrared laser heating system: Application to the Earth's deep interior. *Phys. Earth Planet. Inter.* **In Press, Corrected Proof**.

Murakami, M., K. Hirose, K. Kawamura, N. Sata and Y. Ohishi (2004). Post-perovskite phase transition in $MgSiO_3$. *Science* **304**: 855-858.

Murakami, M., Y. Ohishi, N. Hirao and K. Hirose (2009). Elasticity of MgO to 130 GPa: Implications for lower mantle mineralogy. *Earth Planet. Sci. Lett.* **277**: 123-129.

Murakami, M., S. V. Sinogeikin, J. D. Bass, N. Sata, Y. Ohishi and K. Hirose (2007a). Sound velocity of $MgSiO_3$ post-perovskite phase; a constraint on the D" discontinuity. *Earth Planet. Sci. Lett.* **259**: 18-23.

Murakami, M., S. V. Sinogeikin, H. Hellwig, J. D. Bass and J. Li (2007b). Sound velocity of $MgSiO_3$ perovskite to Mbar pressure. *Earth Planet. Sci. Lett.* **256**: 47-54.

Murnaghan, F. D. (1937). *Am J Math* **49**: 235.

Musgrave, M. J. P. (1970). *Crystal Acoustics: Introduction to the Study of Elastic Waves and Vibrations in Crystals*. San Francisco, Holden-Day.

Newnham, R. E. (2005). *Properties of Materials: Anisotropy, Symmetry, Structure*, Oxford University Press.

Nguyen, J. H. and N. C. Holmes (2004). Melting of iron at the physical conditions of the Earth's core. *Nature* **427**: 339-342.

Nye, J. (1985). *Physical Properties of Crystals*. Oxford, Clarendon Press.

Oganov, A. R. and S. Ono (2004). Theoretical and experimental evidence for a post-perovskite phase of $MgSiO_3$ in Earth's D" layer. *Nature* **430**: 445-448.

Panning, M. and B. Romanowicz (2004). Inferences on Flow at the Base of Earth's Mantle Based on Seismic Anisotropy. *Science* **303**: 351-353.

Panning, M. and B. Romanowicz (2006). A three-dimensional radially anisotropic model of shear velocity in the whole mantle. *Geophys. J. Int.* **167**: 361-379.

Papagelis, K. and S. Ves (2003). Vibrational properties of the rare earth aluminum garnets. *J. Appl. Phys.* **94**: 6491-6498.

Persson, K., A. Bengtson, G. Ceder and D. Morgan (2006). Ab initio study of the composition dependence of the pressure-induced spin transition in the $(Mg_{1-x}Fe_x)O$ system. *Geophys. Res. Lett.* **33**: L16306.

Poirier, J.-P. (1991). *Introduction to the Physics of the Earth's Interior*, Cambridge University Press.

Polian, A. (2003). Brillouin scattering at high pressure: an overview. *J. Raman Spectrosc.* **34**: 633-637.

Reichmann, H. J., S. D. Jacobsen, S. J. Mackwell and C. A. McCammon (2000). Sound wave velocities and elastic constants for magnesiowustite using gigahertz interferometry. *Geophys. Res. Lett.* **27**: 799-802.

Reichmann, H. J., S. V. Sinogeikin and J. D. Bass (2008). Single-crystal elastic properties of $(Mg_{0.987}Fe_{0.013})O$ to 9 GPa. *Am. Mineral.* **93**: 1306-1311.

Reuss, A. (1929). Berechnung der Fließgrenze von Mischkristallen aufgrund der Konstanten des Einkristalls. *Zeit. Angew. math. Meth.* **92**: 49.

Ringwood, A. E. (1975). *Composition and Petrology of the Earth's Mantle*. New York, McGraw-Hill.

Romanowicz, B. (2008). Using seismic waves to image Earth's internal structure. *Nature* **451**: 266-268.

Sandercock, J. R., Ed. (1982). *Trends in Brillouin scattering: studies of opaque materials, supported films, and central modes.* Light scattering in solids III: recent results, topics in applied physics. Berlin, Springer.

Schilling, F. R., M. Hauser, S. V. Sinogeikin and J. D. Bass (2001). Compositional dependence of elastic properties and density of glasses in the system anorthite-diopside-forsterite. *Contributions to Mineralogy and Petrology* **141**: 297-306.

Schuh, L., R. Metselaar and C. R. A. Catlow (1991). Computer modelling studies of defect structures and migration mechanisms in yttrium aluminium garnet. *J. Eur. Ceram. Soc.* **7**: 67-74.

Shannon, R. (1976). Revised effective ionic radii and systematic studies of interatomic distances in halides and chalcogenides. *Acta Crystallogr. Sec. A* **32**: 751-767.

Shimizu, H., H. Imaeda, T. Kume and S. Sasaki (2005). High-pressure elastic properties of liquid and solid neon to 7 GPa. *Phys. Rev. B* **71**: 014108-014105.

Sinogeikin, S., J. Bass, V. Prakapenka, D. Lakshtanov, G. Shen, C. Sanchez-Valle and M. Rivers (2006). Brillouin spectrometer interfaced with synchrotron radiation for simultaneous x-ray density and acoustic velocity measurements. *Rev. Sci. Instrum.* **77**: 103905-103911.

Sinogeikin, S. V. and J. D. Bass (2000). Single-crystal elasticity of pyrope and MgO to 20 GPa by Brillouin scattering in the diamond cell. *Phys. Earth Planet. Inter.* **120**: 43-62.

Sinogeikin, S. V. and J. D. Bass (2002a). Elasticity of majorite and a majorite-pyrope solid solution to high pressure; implications for the transition zone. *Geophys. Res. Lett.* **29**: 1017.

Sinogeikin, S. V. and J. D. Bass (2002b). Elasticity of pyrope and majorite-pyrope solid solutions to high temperatures. *Earth Planet. Sci. Lett.* **203**: 549-555.

Sinogeikin, S. V., J. D. Bass and T. Katsura (2003). Single-crystal elasticity of ringwoodite to high pressures and high temperatures: implications for 520 km seismic discontinuity. *Phys. Earth Planet. Inter.* **136**: 41-66.

Sinogeikin, S. V., J. M. Jackson, B. O'Neill, J. W. Palko and J. D. Bass (2000). Compact high-temperature cell for Brillouin scattering measurements. *Rev. Sci. Instrum.* **71**: 201-206.

Sinogeikin, S. V., D. L. Lakshtanov, J. D. Nicholas and J. D. Bass (2004a). Sound velocity measurements on laser-heated MgO and Al_2O_3. *Phys. Earth Planet. Inter.* **143-144**: 575-586.

Sinogeikin, S. V., D. L. Lakshtanov, V. B. Prakapenka, C. Sanchez-Valle, J. Wang, B. Chen, G. Shen and J. D. Bass (2007). Toward a self-consistent pressure scale: elastic moduli and equation of state of MgO by simultaneous x-ray density and Brillouin sound velocity measurements at high-pressure high-temperature conditions. *Eos Trans., AGU* **88**: Fall Meet. Suppl., Abstract MR53A-07.

Sinogeikin, S. V., J. Zhang and J. D. Bass (2004b). Elasticity of single crystal and polycrystalline $MgSiO_3$ perovskite by Brillouin spectroscopy. *Geophys. Res. Lett.* **31**: L06620.

Slater, J. C. (1963). *Introduction to Chemical Physics*. New York, McGraw-Hill.

Speziale, S. and T. S. Duffy (2004). Single-crystal elasticity of fayalite to 12 GPa. *J. Geophys. Res.* **109**: B12202.

Speziale, S., V. E. Lee, S. M. Clark, J. F. Lin, M. P. Pasternak and R. Jeanloz (2007a). Effects of Fe spin transition on the elasticity of (Mg,Fe)O magnesiowüstite and implications for the seismological properties of the Earth's lower mantle. *J. Geophys. Res.* **112**.

Speziale, S., A. Milner, V. E. Lee, S. M. Clark, M. P. Pasternak and R. Jeanloz (2005). Iron spin transition in Earth's mantle. *Proc. Natl. Acad. Sci.* **102**: 17918-17922.

Speziale, S., H. J. Reichmann, H. Marquardt and F. R. Schilling (2007b). A new Brillouin Spectroscopy laboratory for the study of minerals and high pressure and temperature. *EGU General Assembly*: 15-20 April, Vienna (Austria).

Speziale, S., S. R. Shieh and T. S. Duffy (2006). High-pressure elasticity of calcium oxide; a comparison between Brillouin spectroscopy and radial X-ray diffraction. *J. Geophys. Res.* **111**: B02203.

Stacey, F. D. (1977). A thermal model of the Earth. *Phys. Earth Planet. Inter.* **15**: 341-348.

Stacey, F. D. (1992). *Physics of the Earth*, Brookfield Press, Queensland.

Stackhouse, S., J. P. Brodholt and G. D. Price (2006). Elastic anisotropy of $FeSiO_3$ end-members of the perovskite and post-perovskite phases. *Geophys. Res. Lett.* **33**: L01304.

Stackhouse, S., J. P. Brodholt and G. D. Price (2007). Electronic spin transitions in iron-bearing $MgSiO_3$ perovskite. *Earth Planet. Sci. Lett.* **253**: 282-290.

Stackhouse, S., J. P. Brodholt, J. Wookey, J. M. Kendall and G. D. Price (2005). The effect of temperature on the seismic anisotropy of the perovskite and post-perovskite polymorphs of $MgSiO_3$. *Earth Planet. Sci. Lett.* **230**: 1-10.

Stixrude, L. and C. Lithgow-Bertelloni (2005). Thermodynamics of mantle minerals - I. Physical properties. *Geophys. J. Int.* **162**: 610-632.

Stixrude, L. and C. Lithgow-Bertelloni (2007). Influence of phase transformations on lateral heterogeneity and dynamics in Earth's mantle. *Earth Planet. Sci. Lett.* **263**: 45-55.

Sturhahn, W. (2004). Nuclear resonant spectroscopy. *J. Phys.: Condens. Matter* **16**: S497-S530.

Sturhahn, W., J. M. Jackson and J.-F. Lin (2005). The spin state of iron in minerals of Earth's lower mantle. *Geophys. Res. Lett.* **32**: L12307.

Su, W.-j. and A. M. Dziewonski (1997). Simultaneous inversion for 3-D variations in shear and bulk velocity in the mantle. *Phys. Earth Planet. Inter.* **100**: 135-156.

Sumino, Y., O. L. Anderson and I. Suzuki (1983). Temperature coefficients of elastic constants of single crystal MgO between 80 and 1,300 K. *Phys. Chem. Miner.* **9**: 38-47.

Tange, Y., E. Takahashi, Y. Nishihara, K.-i. Funakoshi and N. Sata (2009). Phase relations in the system MgO-FeO-SiO_2 to 50 GPa and 2000 °C: An application of experimental techniques using multianvil apparatus with sintered diamond anvils. *J. Geophys. Res.* **114**: B02214.

Thurber, C. and J. Ritsema (2007). Seismic Tomography and Inverse Methods. *Treatise in Geophysics - Seismology and Structure of the Earth*. B. Romanowicz and A. Dziewonski. Amsterdam, Elsevier.

Tsuchiya, T., R. Wentzcovitch, C. da Silva, S. de Gironcoli and J. Tsuchiya (2006a). Pressure induced high spin to low spin transition in magnesiowüstite. *Phys. Status Solidi B* **243**: 2111-2116.

Tsuchiya, T., R. M. Wentzcovitch, C. R. S. da Silva and S. de Gironcoli (2006b). Spin transition in magnesiowüstite in Earth's lower mantle. *Phys. Rev. Lett.* **96**: 198501-198504.

Umemoto, K., R. M. Wentzcovitch, Y. Yu and R. Requist (2008). Spin transition in ferrous iron in $MgSiO_3$ perovskite under pressure. *Eos Trans. AGU* **89**: Fall Meet. Suppl., Abstract MR31A-1824.

Utsumi, W., N. Toyama, S. Endo, F. E. Fujita and O. Shimomura (1986). X-ray diffraction under ultrahigh pressure generated with sintered diamond anvils. *J. Appl. Phys.* **60**: 2201-2204.

Vinnik, L., L. Breger and B. Romanowicz (1998). Anisotropic structures at the base of the Earth's mantle. *Nature* **393**: 564-567.

Voigt, W. (1928). *Lehrbuch der Kristallphysik*, Teubner, Berlin.

Walte, N. P., F. Heidelbach, N. Miyajima, D. J. Frost, D. C. Rubie and D. P. Dobson (2009). Transformation textures in post-perovskite: Understanding mantle flow in the D" layer of the Earth. *Geophys. Res. Lett.* **36**: L04302.

Wang, J., S. Sinogeikin, T. Inoue and J. D. Bass (2006). Elastic properties of hydrous ringwoodite at high-pressure conditions. *Geophys. Res. Lett.* **33**: L14308.

Wang, Z. and S. Ji (2001). Elasticity of six polycrystalline silicate garnets at pressure up to 3.0 GPa. *Am. Mineral.* **86**: 1209-1218.

Watt, J. P. (1988). Elastic properties of polycrystalline minerals: Comparison of theory and experiment. *Phys. Chem. Miner.* **15**: 579-587.

Weidner, D. J., J. D. Bass, A. E. Ringwood and W. Sinclair (1982). The Single-Crystal Elastic Moduli of Stishovite. *J. Geophys. Res.* **87**: 4740–4746.

Wenk, H. R., S. Speziale, A. K. McNamara and E. J. Garnero (2006). Modeling lower mantle anisotropy development in a subducting slab. *Earth Planet. Sci. Lett.* **245**: 302-314.

Wentzcovitch, R. M., B. B. Karki, M. Cococcioni and S. de Gironcoli (2004). Thermoelastic Properties of $MgSiO_3$-Perovskite: Insights on the Nature of the Earth's Lower Mantle. *Phys. Rev. Lett.* **92**: 018501.

Wentzcovitch, R. M., T. Tsuchiya and J. Tsuchiya (2006). $MgSiO_3$ postperovskite at D" conditions. *Proc. Natl. Acad. Sci.* **103**: 543-546.

Whitfield, C. H., E. M. Brody and W. A. Bassett (1976). Elastic moduli of NaCl by Brillouin scattering at high pressure in a diamond anvil cell. *Rev. Sci. Instrum.* **47**: 942-947.

Wilson, M. and P. F. McMillan (2004). Interpretation of x-ray and neutron diffraction patterns for liquid and amorphous yttrium and lanthanum aluminum oxides from computer simulation. *Phys. Rev. B* **69**: 054206.

Wookey, J., S. Stackhouse, J. M. Kendall, J. Brodholt and G. D. Price (2005). Efficacy of the post-perovskite phase as an explanation for lowermost-mantle seismic properties. *Nature* **438**: 1004-1007.

Yagi, T. and S.-I. Akimoto (1976). Direct determination of coesite- stishovite transition by in-situ X-ray measurements. *Tectonophysics* **35**: 259-270.

Yamazaki, D. and S.-i. Karato (2001). Some mineral physics constraints on the rheology and geothermal structure of Earth's lower mantle. *Am. Mineral.* **86**: 385-391.

Yamazaki, D. and S.-i. Karato (2002). Fabric development in (Mg,Fe)O during large strain, shear deformation: implications for seismic anisotropy in Earth's lower mantle. *Phys. Earth Planet. Inter.* **131**: 251-267.

Zha, C.-s., T. S. Duffy, R. T. Downs, H.-K. Mao and R. J. Hemley (1996). Sound velocity and elasticity of single-crystal forsterite to 16 GPa. *J. Geophys. Res.* **101**: 17,535-517,545.

Zha, C.-s., T. S. Duffy, R. T. Downs, H.-k. Mao and R. J. Hemley (1998). Brillouin scattering and X-ray diffraction of San Carlos olivine: direct pressure determination to 32 GPa. *Earth Planet. Sci. Lett.* **159**: 25-33.

Zha, C.-s., T. S. Duffy, H.-k. Mao, R. T. Downs, R. J. Hemley and D. J. Weidner (1997). Single-crystal elasticity of beta-Mg_2SiO_4 to the pressure of the 410 km seismic discontinuity in the Earth's mantle. *Earth Planet. Sci. Lett.* **147**: E9-E15.

Zha, C.-s., H.-k. Mao and R. J. Hemley (2000). Elasticity of MgO and a primary pressure scale to 55 GPa. *Proc. Natl. Acad. Sci.* **97**: 13494-13499.

Zhang, S. and S.-i. Karato (1995). Lattice preferred orientation of olivine aggregates deformed in simple shear. *Nature* **375**: 774-777.

Chapter 6.1

This chapter is submitted as

"Single-Crystal Elastic Properties of $(Mg_{0.9}Fe_{0.1})O$ to 81 GPa" (*Earth and Planetary Science Letters*, 2009)

by

Hauke Marquardt, Sergio Speziale, Hans J. Reichmann, Daniel J. Frost, Frank R. Schilling

This chapter is not included in the online version, but will be available online at:

http://www.elsevier.com/wps/find/journaldescription.cws_home/503328/description#description

Chapter 6.2

This chapter is published as

“Elastic Shear Anisotropy of Ferropericlase in Earth’s Lower Mantle” (*Science* 324, 224-226, 2009)

by

Hauke Marquardt, Sergio Speziale, Hans J. Reichmann, Daniel J. Frost, Frank R. Schilling, Edward J. Garnero

This chapter is not included in the online version, but is available online at:

http://dx.doi.org/10.1126/science.1169365

Chapter 6.3

This chapter is submitted as

“Single-Crystal Elastic Properties of $(Y,Yb)_3Al_5O_{12}$”

(*Journal of Applied Physics*, 2009)

by

Hauke Marquardt, Sergio Speziale, Sandro Jahn, Steffen Ganschow, Frank R. Schilling

This chapter is not included in the online version, but will be available online at:

http://jap.aip.org/

Appendix

AI. Zusammenfassung

Elastische Eigenschaften bestimmen die Reaktion von Materialen auf Verformungen innerhalb des elastischen Bereichs. Sie spiegeln die Natur der atomaren Bindungen (Stärke) wider und geben Auskunft über die physikalischen und chemischen Eigenschaften von Materialien - das begründet das große Interesse an Elastizität von zahlreichen wissenschaftlichen Disziplinen, unter anderem Materialwissenschaften, Festkörperphysik, Geowissenschaften und Chemie. In den Geowissenschaften gibt es ein besonderes Interesse am Verständnis der elastischen Eigenschaften der Minerale die im Erdinneren vorkommen, weil sie das Ausbreitungsverhalten von seismischen Wellen in unserem Planeten bestimmen. Ein quantitatives Verständnis von elastischen Wellengeschwindigkeiten in Mineralen unter den extremen Bedingungen des Erdinneren ermöglicht die Interpretation von seismologischen Beobachtungen und wird für ein besseres Verständnis der Zusammensetzung, Entwicklung, Dynamik und Temperaturverteilung im tiefen Erdinneren benötigt. Die vorliegende Arbeit trägt zu diesem Ziel bei, indem sie sich mit der Abhängigkeit elastischer Eigenschaften von der chemischen Zusammensetzung, dem Druck und der Temperatur befasst.

Kapitel 2 stellt eine kurze Einführung in die Struktur, Mineralogie, Dynamik und den Wärmehaushalt des tiefen Erdinneren dar und erläutert die Motivation für diese Arbeit. Kapitel 3 beschäftigt sich mit der Elastizitätstheorie und fasst wichtige Zusammenhänge zwischen elastischen Eigenschaften und der Ausbreitung von Schallwellen in Einkristallen und Mineralaggregaten zusammen. Die Beschreibung von elastischen Eigenschaften im Rahmen der finiten Verformungstheorie wird ebenfalls kurz erläutert. Dieses Kapitel schließt mit einer Kurzdarstellung der Methoden ab, die am Häufigsten zur Elastizitätsbestimmung bei hohem Druck und hoher Temperatur verwendet werden. Kapitel 4 stellt die experimentellen Methoden vor, die in dieser Arbeit verwendet wurden. Zunächst wird das Wirkungsprinzip von Diamantstempelzellen zur Erzeugung der hohen Drücke des Erdinneren erläutert. Anschließend werden die beiden Meßmethoden erklärt, die in dieser Arbeit vorrangig benutzt wurden: Brillouin Streuung und Röntgendiffraktion.

Die Ergebnisse dieser Arbeit werden in Kapitel 5 und 6 diskutiert. Die wichtigsten Resultate und Implikationen sind in Form von erweiterten Zusammenfassungen dargelegt (Kapitel 5) und werden dabei durch die kompletten Manuskripte ergänzt (Kapitel 6).

Der erste Teil (5.1, 5.2, 5.3) der Diskussion beschäftigt sich mit der Druck-, Temperatur- und Zusammensetzungsabhängigkeit der elastischen Eigenschaften von einkristallinem (Mg,Fe)O Ferroperiklas, dem zweithäufigsten Mineral des unteren Erdmantels. Es konnte kürzlich gezeigt werden, dass das sechsfach koordinierte zweiwertige Eisen im Ferroperiklas bei Drücken des unteren Mantels einen Spin-Übergang durchläuft, welcher von Änderungen in zahlreichen physikalischen Eigenschaften, einschließlich Elastizität, begleitet ist.

Kapitel 5.1 diskutiert den Effekt dieses druck-induzierten Spin-Übergangs auf die elastischen Eigenschaften von Ferroperiklas und die Bedeutung für die Interpretation von sowohl eindimensionalen als auch dreidimensionalen seismologischen Modellen. Das wichtigste Ergebnis ist, dass der Spin-Übergang die Geschwindigkeiten der Kompressionswellen stark verringert, aber keinen Einfluss auf die Scherwellen hat. Das führt zu einer ausgeprägten Veränderung der Geschwindigkeitsverhältnisse und deren Abhängigkeit von Druck, Temperatur und Eisengehalt. Wenn diese Mechanismen gut verstanden sind, und wenn zukünftige, zielgerichtete seismologische Studien die elastische Signatur des Spin-Übergangs erfolgreich auflösen, dann kann der Spin-Übergang wichtige Informationen über die Temperatur- und Eisenverteilung im mittleren unteren Mantel liefern (Marquardt et al. 2009b).

Kapitel 5.2 erläutert die Bedeutung von (Mg,Fe)O für die Interpretation von seismischen Anisotropie-Beobachtungen im tiefen unteren Mantel. Das wichtigste Resultat ist, dass (Mg,Fe)O Ferroperiklas wahrscheinlich die elastische Anisotropie im unteren Mantel dominiert, obwohl es nur etwa 20 Vol. % dieser Region ausmacht. Diese Daten implizieren, dass seismische Anisotropie auch oberhalb der D'' Diskontinuität, wo Seismologen sie beobachten, vorhanden sein könnte - in Regionen, in denen die Deformation durch Dislokationskriechen bei sehr hohen Verformungsraten gekennzeichnet ist. Diese Erkenntnisse können von großer Bedeutung für unser Verständnis von Mantelkonvektion und die Dynamik der Erde sein (Marquardt et al. 2009c).

Kapitel 5.3 diskutiert den Temperatureffekt auf die elastischen Konstanten von (Mg,Fe)O bei hohen Drücken. Die Ergebnisse zeigen, dass eine Erhöhung der Temperatur im Allgemeinen zu geringeren elastischen Geschwindigkeiten führt, aber auch deutlich die elastische Scherwellen-Anisotropie beeinflusst. Eine Erhöhung der Temperatur führt zu einer

stärkeren elastischen Anisotropie bei Drücken unter ~20 GPa, verringert aber die Anisotropie bei den Drücken des unteren Mantels. Diese ersten Ergebnisse zu den elastischen Eigenschaften von Ferroperiklas bei hohem Druck und hoher Temperatur stellen eine Grundlage für zukünftige Arbeiten zur experimentellen Quantifizierung der elastischen Eigenschaften unter den Bedingungen des Erdmantels dar.

Der zweite Teil dieser Arbeit (5.4, 5.5) beschäftigt sich mit dem Einfluss von chemischer Substitution auf den elastischen Tensor von synthetischen und natürlichen Granatmischreihen. Silikatgranate sind Hauptbestandteile in der Erdkruste und dem oberen Erdmantel, vor allem in der Übergangszone. Außerdem sind Kristalle der Granatgruppe wichtige Verbindungen in die Materialwissenschaften, da sie für eine Reihe von technischen Anwendungen geeignet sind, beispielsweise als Festkörperlaser.

Kapitel 5.4 diskutiert die elastischen Eigenschaften von synthetischen Granaten der Mischreihe $Y_3Al_5O_{12}$-$Yb_3Al_5O_{12}$, die sowohl mit Brillouin Spektroskopie als auch mit Computersimulationen bestimmt wurden. Die Daten zeigen, dass die Substitution von Yttrium mit dem kleineren und schwereren Ytterbium das Material steifer macht (die Inkompressibilität nimmt zu), aber keinen Effekt auf die Schereigenschaften hat. Diese Erkenntnisse können zu einem besseren Verständnis von Elastizitäts-Zusammensetzungs-Systematiken in natürlichen Granaten und den Potentialen und Grenzen von Computersimulationen beitragen (Marquardt et al. 2009a).

Kapitel 5.5 beschäftigt sich mit den elastischen Eigenschaften von natürlichen Granaten und vergleicht sie zu der Systematik, die für die synthetischen Mischkristallreihen beobachte wurde. Das Hauptergebnis ist, dass die untersuchten natürlichen Granate analog auf die Substitution von Kationen reagieren – die Inkompressibilität ändert sich, aber die Schereigenschaften bleiben unverändert. Diese Beobachtungen legen nahe, dass die Elastizitäts-Systematik, zumindest bis zu einem gewissen Grad, übertragbar ist auf verschiedene Granatmischreihen und möglicherweise auch auf Majorit-Pyrop Granat, der wahrscheinlich häufigsten einzelnen Mineralphase in der Übergangszone, zutrifft.

AII. Erklärung

Hiermit versichere ich, dass die vorliegende Arbeit selbstständig verfasst und keine anderen als die angegebenen Hilfsmittel benutzt habe. Die Stellen der Arbeit, die anderen Werken wörtlich oder inhaltlich entnommen sind, wurden durch entsprechende Angaben der Quellen kenntlich gemacht.

Diese Arbeit hat in gleicher oder ähnlicher Form noch keiner Prüfungsbehörde vorgelegen.

Berlin, 30.04.09, Hauke Marquardt

AIII. Lebenslauf

Der Lebenslauf ist in der Online-Version aus Gründen des Datenschutzes nicht enthalten